Advances in Liquid Metal Printed 2D Oxide Electronics

William J. Scheideler[1]* *and Kenji Nomura*[2]

[1]Thayer School of Engineering
Dartmouth College, Hanover, NH 03755, United States
E-mail: william.j.scheideler@dartmouth.edu

[2]Department of Electrical and Computer Engineering,
University of California San Diego, La Jolla, CA 92093, United States;

Keywords: *liquid metal printing, 2D oxides, metal oxide semiconductors, transparent electronics*

Abstract

Two-dimensional metal oxides (2DMOs) have recently emerged as a high-performance class of ultrathin, wide bandgap materials offering exceptional electrical and optical properties for a wide area of device applications in energy, sensing, and display technologies. Liquid metal printing represents a thermodynamically advantageous strategy for synthesizing 2DMOs by a solvent-free and vacuum-free scalable method. Here, we review recent progress in the field of liquid metal printed 2D oxides, considering how the physics of Cabrera-Mott oxidation gives this rapid, low-temperature process advantages over alternatives such as sol-gel and nanoparticle processing. We analyze the growth, composition, and crystallinity of a burgeoning set of 1-3 nm thick liquid metal printed semiconducting, conducting, and dielectric oxides that are uniquely suited for the fabrication of high-performance flexible electronics. We consider the advantages and limitations of these strategies, highlighting opportunities to amplify the impact of 2DMO through large area printing, the design of doped metal alloys, stacking of 2DMO to electrostatically engineer new oxide heterostructures, and implementation of 2D oxide devices for gas sensing, photodetection, and neuromorphic computing.

1. Introduction

The thin surface oxide skin of liquid metals has recently been discovered to be a powerful and versatile synthetic tool[1] for manufacturing 2D materials with device applications spanning energy, sensing, and thin film electronics. This growing class of 2D metal oxide (2DMO) nanomaterials (In_2O_3, SnO, ZnO, PbO, Al_2O_3, CoO_x, Ga_2O_3, MnO_x, TeO_2, etc.) has unique properties unachievable in bulk films that are induced by its thickness at the single nm scale, including outstanding mechanical flexibility[2], rapid gas sensing response[3], enhanced piezoelectricity[4], and high surface area[5]. For example, 2D oxides with thicknesses below the Bohr Radius (a_B ~ 2-3 nm for In_2O_3, ZnO, SnO_2, etc.) exhibit extreme transparency afforded by their quantum-induced widened optical bandgap[6]. Furthermore, they can exhibit high crystallinity with unique overlapping morphologies of large crystal grains[7–9] rarely found in vacuum deposited films. Another rare, unexpected property is the highly efficient hole transport that has been observed in p-type 2D oxides such as β-TeO_2[10] and SnO[11], which can provide opportunities for designing complementary circuits (CMOS) for next-generation sustainable electronics with low power dissipation.

Many of these outstanding properties of 2DMOs derive from the exceptional physics of liquid metal surface oxidation. In this synthetic method, native oxidation of the liquid metal surface at low temperatures (e.g. < 200 ˚C) or even room temperature[12] leads to the growth of a solid surface oxide approximately 0.5 - 3 nm thick that can be transferred to a target surface via Van der Waals adhesion. For many transition metals, this oxidation process proceeds rapidly, regenerating the surface oxide layer at the millisecond time scale as the liquid metal meniscus is deformed. The greater promise of these materials in thin film electronics rests on two major advantages of these liquid metal synthetic methods:

1) They could be scaled for large area deposition using printing techniques.
2) The low melting temperature of alloys based on In, Ga, and Sn allows these methods to deposit 2DMOs on flexible substrates within a limited thermal budget[2,13,14].

Roll-based continuous liquid metal printing[13] combines both these advantages and could allow translation to high speeds and compatibility with large scale roll-to-roll (R2R) equipment. Another key distinguishing feature of liquid metal printing is that it is cost-effective because it is vacuum-free, not requiring any expensive equipment that otherwise dominates the manufacturing cost of thin film electronics. The tunable chemistry of 2DMOs presents an opportunity to engineer a new class of ultrathin electronic materials that can be high performance *and* scalable, with extremely simple, low-cost precursors comprising only pure metals and their alloys rather than metalorganic precursors that themselves require complex synthesis and expensive purification.

This review focuses on liquid metal printed 2DMOs, exploring how this new approach can become a tool for fabricating high performance oxide electronic devices based on 2D oxides. The scope of this review is depicted in **Figure 1**, showing the examination of interrelated topics spanning fabrication, electronic properties of 2DMOs, and device design and applications. The physics of surface oxidation, fluid mechanics liquid metal printing, and the growth kinetics of 2DMOs will be explored to understand the capabilities and limitations of this technology. Control of film thickness and crystalline phase at the nanoscale has implications for many electronic and optical properties, including carrier mobility[15], optical bandgap[6], and dielectric properties[16]. We will analyze device applications of these 2DMOs to thin film transistors, photodetectors, and emerging areas such as neuromorphic computing and room temperature gas sensing, mapping their electronic performance as a function of composition and thickness. Finally, we examine challenges for scaling and advancing these device technologies as well as synthetic opportunities for transforming 2DMOs into 2D materials such as nitrides, sulfides[17], phosphides, and phosphates[18]with exceptional optoelectronic properties and high electron mobility above 200 cm^2/Vs[19].

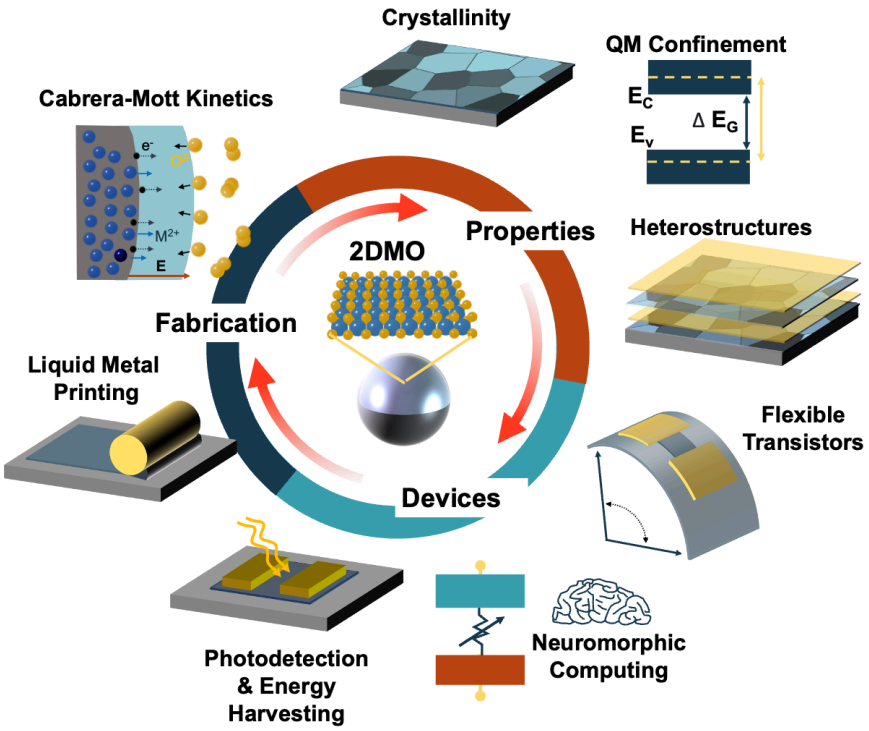

***Figure 1**: Schematic depicting topics of active research in fabrication, electronic properties, and device applications of two-dimensional metal oxides (2DMOs) synthesized from liquid metal interfaces.*

Results and Discussion

2 – Synthesis, Processing, and Properties of Liquid Metal Printed 2D Metal Oxides

To build a deeper, more coherent understanding of the field of 2D metal oxides (2DMOs), we begin by reviewing their fabrication and then consider their physical properties such as their thickness and their crystallinity. The starting point for making 2DMOs is a metal in its liquid phase in an oxidizing atmosphere, for example, pure molten indium in air. This quantity of indium metal spontaneously grows a native, nanometer-scale thick surface oxide regardless of whether it is below or above its melting temperature of 156.6 ºC, however, the subsequent steps of transferring or 'printing' the 2D surface oxide depend on maintaining the liquid phase. As discussed in the following sections, research on 2DMOs has developed methods for controlling the surface oxidation and printing processes to produce high-quality films at technologically relevant speeds over large areas (**Section 2.1-2.3**). The nanoscale morphology, chemical composition, and physical properties that result from 2DMO printing methods derive from the physics of the Cabrera Mott oxidation process, as will be discussed in **Sections 2.4-2.6**.

2.1 Fundamentals of Large Area 2D Metal Oxide Printing

Liquid metal printing (LMP) of 2D oxides represents a fundamentally different approach compared to other solution-processed materials such as sol-gel methods and nanoparticles due to its use of spontaneous oxidation that can process 2DMOs at the single second time scale[20]. LMP is fundamentally a *dry*, *solvent-free* method that eliminates the need for toxic volatile chemicals such as 2-methoxyethanol[21] that are widely used across printed inorganic electronics based on sol-gels. Additionally, the spontaneous surface oxidation of 2D oxides is thermodynamically favorable, eliminating the need for slow, high temperature annealing steps that are necessary to densify sol-gel materials after deposition. Nanoparticle synthesis performs this high temperature calcination step before the fluid ink is formulated, but an important consequence is that electrical conductivity and mobility of nanoparticulate films suffer due to poor interparticle transport when foregoing high temperature sintering[22].

2D oxides, on the other hand, allow the printing of large area films that are highly continuous and free of any macroscopic pinhole defects over cm^2 areas[2,13,20,24,25] despite their ultrathin nature (1-3 nm thick). This property is unique compared with other 2D materials such as graphene and MoS_2, for which solution-phase exfoliation and adhesive transfer are limited to relatively small flake sizes in the range of tens of μm[26]. 2DMO printing demonstrated in the literature has included several distinct methods for manipulating liquid metal droplets by pressing, scraping, and rolling.

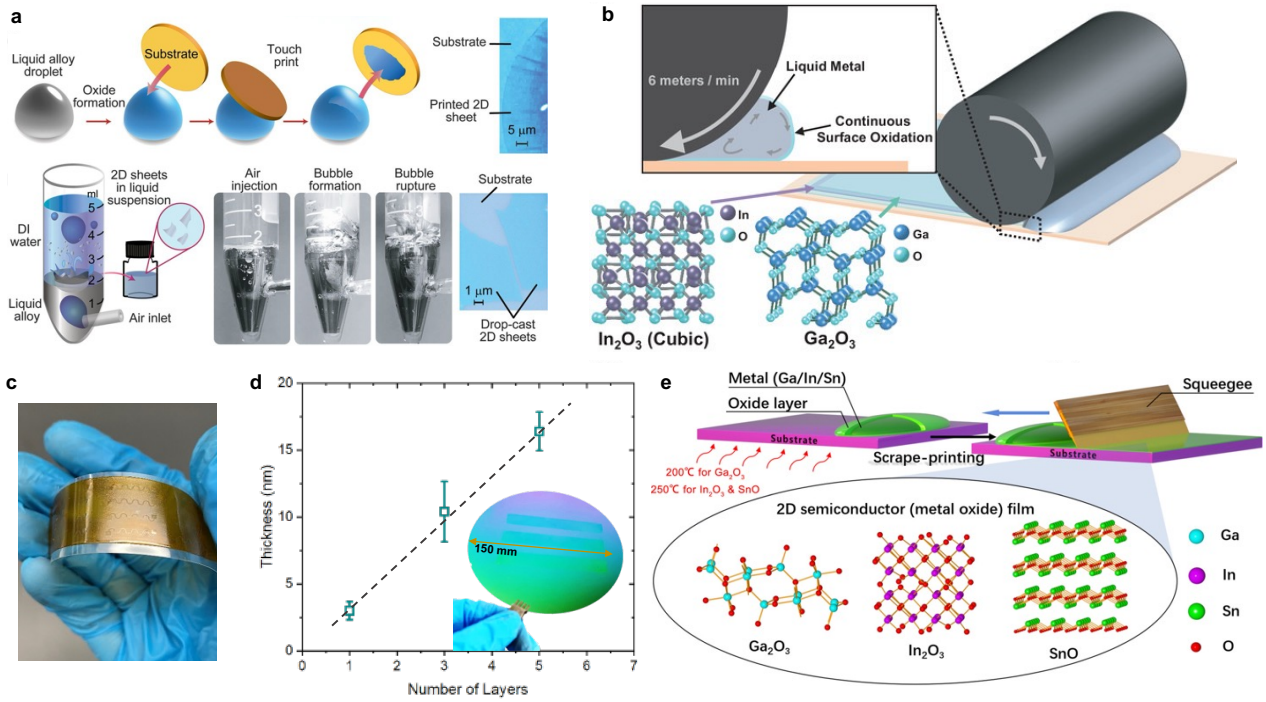

***Figure 2**: Summary of liquid metal synthesis and deposition methods including touch printing and liquid exfoliation (a)[12], continuous liquid metal printing (CLMP) (b-d)[23], and squeegee-based scrape printing (e) [24]. (c,d) show images of resulting large area films formed by printing layers of 2D Ga_2O_3 and In_2O_3 using continuous liquid metal printing (CLMP)[23].*

In 2017, Zavabeti et al. introduced a touch printing method (**Figure 2a**) for transferring the metal oxide skin via a manual pressing process between two substrates[12] in addition to a method for synthesizing solutions of metal oxide nanosheet inks. The touch printing method specifically has been widely reproduced by a number of groups, with one of its greatest advantages being its simplicity and its capability for synthesizing a large variety of 2DMOs based on new metal precursor alloys in various oxidative environments (open air or in a controlled glovebox atmosphere). However, one relative disadvantage regarding scaling up the area and repeatability of this method is that it is fundamentally a batch-wise process based on the spreading of a small molten metal droplet. Most works utilizing these methods demonstrate films with diameters of only a few mm.

To resolve the low areal throughput and limited reliability of previous sequential methods for liquid metal printing based on the deformation of individual droplets, we have reported a roller-based, continuous liquid metal printing (CLMP), as shown in **Figure 2b**. Using this method, oxidation and transfer of 2DMOs can be performed simultaneously at high speeds (> 6 meters/minute) while producing highly uniform In_2O_3 and Ga_2O_3 films as well as complex heterostructures[7]. Even single-layer films printed at high speeds by CLMP can be highly continuous, offering efficient transport and high mobility[20] over large areas. The uniform layer

generation over wafer-scale areas on rigid and flexible substrates (**Figure 2c,d**) greater than 100 cm^2 can be accomplished with only angstroms-level variation in thickness across this scale. **Figure 2e** shows another popular method demonstrated by Li, et al., which uses a squeegee to draw the liquid metal meniscus in a continuous fashion[24]. The authors demonstrate this squeegee printing method for SnO, Ga_2O_3, and In_2O_3, integrating these materials into photodetectors on Si.

In evaluating the state of this field, we might begin by comparing liquid metal printing to alternative methods for oxide film deposition such as solution-processed sol-gels and vacuum deposited oxides. One of the advantages of liquid metal printing is the ability to print ultrathin layers with high uniformity, however, the literature in this field does not yet offer a method to dial in a particular thickness as could be done by tuning solution ink concentration or tuning the deposition time for vacuum processing methods. Enhanced process control and a deeper understanding of the physics of liquid metal printing will be essential if these methods are to overtake incumbent technologies in the future.

To advance towards a larger area method with the potential for inline patterning, past work by Syed et al. illustrated how patterning of the target substrate with regions coated with self-assembled FDTES silane layer allowed selective transfer of 2D Ga_2O_3 (converted to $GaPO_4$) by a blading process akin to screen printing over areas of approximately 1 cm × 4 cm[18], as shown in **Figure 3a**. These blading-based methods have not yet been extended to generate high-resolution patterns at the micron-scale relevant for metal oxide thin film transistors, but there is the possibility

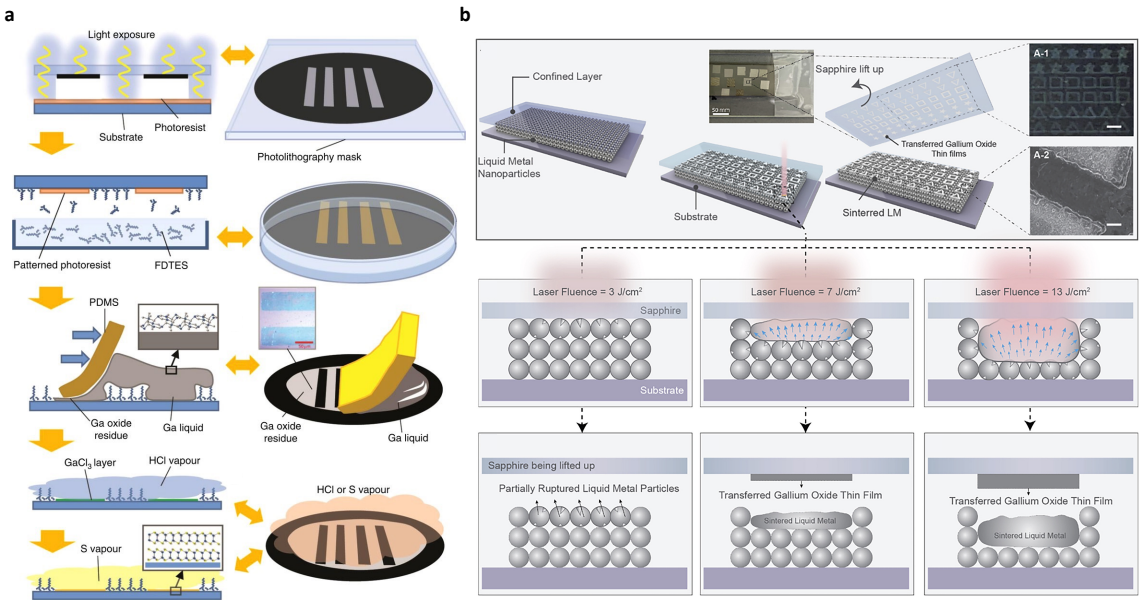

Figure 3*: Summary of reported patterning methods for liquid metal printed 2D oxides including (a) screen printing with self-assembled monolayer surface patterns that modulate the adhesion of 2D Ga_2O_3 and (b) confined laser transfer printing (CLTP). Part a is reproduced from Ref.* [28]*. Part b is reproduced from Ref.* [27].

that they could be combined with additional patterning and deposition schemes. Another advance towards patterning has involved the development of a laser based transfer (**Figure 3b**) ('Confined Laser Transfer Printing – CLTP') demonstrated by An and Cheng in 2023[27], which they apply to directly pattern the formation of 2D Ga_2O_3 films at the micron-scale. This approach uses a confined layer of liquid metal nanodroplets that are simultaneously sintered at which time they transfer their surface oxide layer to the target substrate, leaving patterns limited only by the laser spot size and thickness of the nanoparticle layer. Extending these methods to additional liquid metal alloys could be a promising method for patterning other functional 2D oxides. Finally, another approach offering greater flexibility for integrating liquid metal printed 2DMOs on various substrates has been an indirect method involving printing of 2D Ga_2O_3 onto an intermediate substrate (PPC/PDMS) followed by transfer of the solid 2DMO sheet to a target substrate[29]. Though performed with small scale touch printing, future applications of this indirect transfer could allow the printing of 2DMOs onto thermally, mechanically, or chemically sensitive materials.

2.2 Benchmarking Liquid Metal Printing as a Scalable Deposition Method

The rapid time scales and low temperatures (**Figure 4**) of liquid metal printing are distinguishing characteristics that exceed the limits of solution processing and vacuum deposition methods. The processing speed and temperature are key for multiple reasons, the first of which is that high throughput processing can result in low per unit manufacturing costs that expand the potential application set of 2D oxides into cost-sensitive large area electronics domains[30], for example,

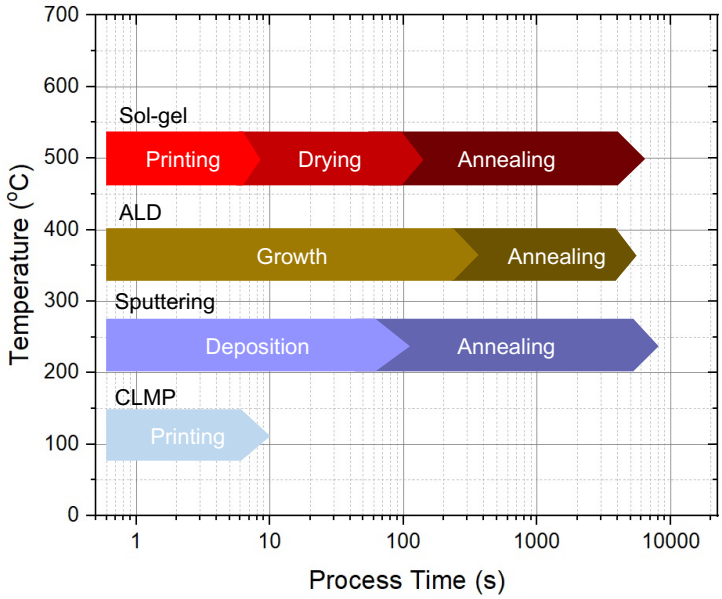

***Figure 4**: Summary comparing temperatures and timescales of metal oxide processing in terms of the deposition as well as annealing and drying times for solution processed films.*

"Giant microelectronics" represented by flat-panel display technology or energy systems such as smart windows and solar cells that are highly driven by cost-metrics. The advantage of 2D liquid metal printing is that the process itself is thermodynamically favorable and the chemistry is simple – there is no need for precursor decomposition as may limit processing of similar materials from metal salt precursors in the case of sol-gels[31]. One result is that 2DMOs processed from liquid metal oxidation do not exhibit significant hydroxide phases, residual nitrates, or carbon impurities otherwise encountered when annealing sol-gel based metal oxides at low temperatures (< 250 C)[32]. For example, we have compared the hydroxide content for 2D In_2O_3 against In_2O_3 sol-gels in past work by evaluating the O1s peak with XPS, finding that even In_2O_3 printed at 160 ºC from liquid metals exhibits far lower hydroxide and increased stoichiometric oxygen bonding[6] compared with sol-gels processed at a similar temperature range.

Figure 4 illustrates the typical process times and temperatures for processing metal oxides from sol-gels, atomic layer deposition (ALD), sputtering, and liquid metal printing (CLMP). Printing can allow sol-gel processing at rapid time scales when applying roll-based methods[33], but the barrier to rapid processing consists of a lengthy drying step that is at least ~ 100 s and often longer, followed by annealing steps that are typically on the order of 1000 – 5000 s (~ 1 hour). These annealing steps at temperatures of 250 – 500 ºC are typically required to achieve high crystallinity and to decompose precursor species consisting of metal salts and residual species from organic solvents[32]. Annealing time can be reduced to 10 – 100 s utilizing ultrathin (< 6 nm) sol-Sol-gel films that can be converted faster to dense, high performance semiconductors, as shown by Wang and Facchetti in 2019[34], however, even the shortest annealing steps achieved in this work required longer pre-annealing drying steps (~ 60 s).

Table 1 details a comparison of the times, temperatures, and vacuum requirements between liquid metal printing, sol-gel processing, and vacuum deposition methods such as sputtering and ALD. High precision vacuum-based chemical vapor deposition growth methods such as ALD based on metal organic precursors can offer similar process temperatures to liquid metal printing of < 200 ºC, but these methods have limitations due to the chamber size for effective pumping and there is a tradeoff encountered for area vs. cycle time vs. uniformity. Sputtering, while scalable to large areas with appropriate target design[35], often requires post deposition annealing steps at higher temperatures (e.g. >300 ºC), for example, to improve the electrical properties of amorphous IGZO. Liquid metal printing instead allows a high degree of electrostatic control (the precise determination of the amount of accumulation layer charge) through the ultrathin channel thicknesses as well as the ability to assemble heterostructures, which can lead to steep switching and high performance without the need for any length post annealing steps[20].

Table 1: *Comparison of process times and temperatures for vacuum deposition, sol-gel, and liquid metal printed metal oxides.*

Method	Vacuum	Precursor	Deposition	Drying	Annealing	Max Temp.
ALD	Yes	*gas* (metalorganic)	10^2–10^3 s	-	~10^3 s	200 - 300 ºC
Sputtering	Yes	*solid*	10^2–10^3 s	-	~10^3 s	200 - 400 ºC
Sol-gel	No	*liquid* (metal salt + solvent)	< 1 s	10^1 - 10^2 s	10^3 – 10^4 s	200 - 500 ºC
Liquid Metal	No	*liquid* (metal)	< 1 s	-	0 - 10 s	40 – 200 ºC

2.3 Fluid Mechanics of Liquid Metal Printing of 2DMOs

Liquid metals present a unique low viscosity fluid system with dynamics dominated by its high surface tension as well as its interactions with solid surfaces – the physics of which are directly linked with the formation and adhesion of solid surface oxides. Rotational viscometry of molten metal viscosity yields measurements that are typically in the range of 1 – 3 cP[36], approximately comparable to the viscosity of water (**Table 2**). However, in contrast with water, molten metals have densities in the range of 6 – 11 g/cm^3 and surface tension of 400 – 715 mN/m, varying with the presence of the surface oxide. Their high surface tension allows method such as continuous liquid metal printing (CLMP) to deform and roll a liquid metal droplet without risk of the droplet spreading uncontrollably (as might happen with an organic solvent or water). **Table 2** summarizes these fluid mechanical properties of low melting temperature metals and their alloys.

The printability of 2DMOs for flexible electronics applications depends on maintaining low melting temperatures of the precursor alloy. An ideal range for making liquid metal printing methods suitable for polyethylene substrates such as PEN and PET is to maintain process temperatures below 200 ºC, above which significant temperature-induced deformation occurs (1-3% strain induced by a 30 minute anneal)[37]. However, we note that substrate deformation is a product of both the temperature and duration of processing, which could suggest the use of rapid, high temperature liquid metal printing steps approaching 250 ºC. Though the melting temperatures of metals such as Sn, Bi, Pb, and Zn exceed the typical liquid metal printing range of RT – 250 ºC (**Table 2**), there is the potential to reduce melting temperatures via formation of eutectic formulations. For example, Sn-Bi eutectic has a T_m of 139 ºC and ternary alloys can reduce this further. Additionally, as discussed in Section 2.2.1, liquid metal alloys composed of small fractions (0-5%) of higher melting temperature metals (e.g. Sb, Al, Hf, etc.) can maintain a low melting temperature[38] in a printable range while facilitating synthesis of a surface oxide dominated by the metal with the more negative redox potential. An important consideration for engineering low

melting temperature precursor alloys to print the oxides of high T_m metals is the role of impurity atoms, which are likely to be incorporated at electronically significant concentrations and distributed non-uniformly in the nanoscale grain structure[39].

The dynamic wetting behavior of liquid metals is also intrinsically linked with the adhesion of the surface oxide to a target substrate, since this behavior dominantly impacts the contact angle hysteresis[40]. In air, liquid metals such as eGaIn exhibit advancing contact angles in the range of 140 – 150 º[40], though when receding, the contact line is pinned by the adhesion of the surface oxide, resulting in a substantial hysteresis above 90º. Joshipura and Dickey have reported that significant surface roughness (RMS > 50 nm) can prevent the oxide adhesion and decrease the pinning of the contact line. Interestingly, this report matches with observations that liquid metal printed 2DMOs transfer ineffectively to substrates such as polyimide with substantial surface roughness[2]. This is perhaps unsurprising given that the 2DMO transfer process is hypothesized to consist of a Van der Waals based adhesion. We note that the challenge of achieving successful Van der Waals transfer of 2D materials to substrates with significant topography has been resolved for materials such as graphene by utilizing viscoelastic transfer stamps to ensure conformal contact[41]. While the thin film mechanics of 2DMOs differ from graphene, there is a chance that similar methods could be applied in combination with future liquid metal printing processes.

Additional methods for surface energy engineering have been reported to aid the assembly of multiple layers of 2DMOs, including interlayer atmospheric pressure plasma treatment[13]. The ability to stack multiple 2DMO layers into heterostructures requires careful consideration of their interfacial adhesion, particularly due to the need to remove the excess metal in between printing steps. Further studies in this area are needed to probe the regimes of time and temperature over which 2DMOs printed via Van der Waals forces can become covalently bonded to each other and to substrates with variable surface chemistries (SiO_2, polyimide, etc.). Deeper mechanical characterization via measurements such as film stress and fracture energy would both be welcome approaches for understanding 2DMOs in this regard.

***Table 2**: Fluid properties including surface tension[42–48], viscosity[45,49], melting temperature, and density[50] of common liquid phase metals. Galinstan = $Ga_{68}In_{20}Sn_{12}$*

Metal	Surface Tension (mN/m)	Viscosity (cP)	T_m (˚C)	Density (g/cm^3)
In	560	1.90	156.6	7.02
Ga	715	1.99	29.8	6.10
eGaIn	625	2.09	15.5	6.25
Galinstan	585	1.81	10.8	6.44
Sn	581	2.61	231.9	6.98
Pb	443	1.63	327.5	10.67
Bi	382	2.60	271.4	10.05

Cd	590	1.90	321.1	8.01

A key factor determining the performance of 2D oxide films is their continuity, which should depend on the dynamics of the liquid metal meniscus. Multiple groups[11,51] have observed that the initial oxide growing on metals such as Sn and other alloys can form a discontinuous island-like morphology of rough oxide 'scale'[52]. This thicker oxide phase is removed before liquid metal printing the desired 2DMOs. To understand the formation of 2D oxide morphologies, we first consider that metals typically exhibit a substantial change in density, and therefore, volume upon their phase transition[53], with most metals expanding after melting (Ga and Bi are the exceptions to this rule). This change in volume can be significant, for example, In exhibits a 2.7 % expansion upon melting[54] while Ga exhibits a 3.1 % contraction[55], which may be translated to strain exerted on the surface oxide. Additionally, molten state metals have a negative dependence of density on temperature, for example, with In expanding by 1.6 % from 164 ºC to 300 ºC[54]. These characteristics would suggest the potential for creating considerable strain in 2DMO films if the printing process involves thermal gradients or mismatched substrate temperatures (e.g. in the case of touch printing). While some recent studies have determined the influence of deposition temperature on electronic properties of 2DMOs[13], further studies are needed to understand how deposition temperature influences the transfer process and the resulting film continuity and uniformity over wafer-scale areas. Transfer from rigid to flexible and stretchable substrates could open new possibilities for 2DMO device applications, but will require engineering suitable adhesion to chemically dissimilar polymer surfaces that are also rougher than the SiO_2 substrates often utilized for previous studies. One recent study has accomplished successful film transfer to stretchable PDMS substrates in the case of 2D $Bi_2O_{2.68}$[56].

Scaling up the speed, area, and resolution of liquid metal printing will require design of automated systems for precisely controlling the shape of the liquid metal meniscus as well as managing the contact pressure. Multiple recent papers have mentioned the need to control contact pressure (e.g. 6-15 N/cm) for consistent transfer of 2DMOs[13,20,24]. These observations suggest that sufficient contact pressure is required to achieve successful transfer, but that excessive pressure during both printing and subsequent wiping steps could risk damaging the printed film or even cracking the substrate (if it is rigid). The challenge of patterning during deposition is familiar to the adjacent field of liquid metal-based stretchable electronics, which has approached this problem via a range of methods[57]. Extrusion based printing offers the ability to pattern small volumes of liquid metal[58], though the process itself utilizes soft contact pressure that may be insufficient for successful 2DMO transfer. Additionally, there is a requirement in the case of metal 2DMO syntheses to have a higher temperature range for printing non-Ga containing alloys. Stencil and screen printing can offer an attractive approach with significant precedent for patterning liquid

metals[57], though adapting these for 2DMO printing would require the ability to remove excess liquid metal without smearing the desired patterns. Reports of ultrasonic bath removal[59] of excess remaining metal are not ideal for large area scalability, but could reduce the smearing effect that a mechanical soft squeegee action would induce. Another approach may be to build off the sensitivity of surface transfer to the surface energy, an issue reported for printing 2DMOs on surfaces such as polymers such as polyethylene and polyimide[13,59]. The sensitivity of 2DMO transfer to surface adhesion suggests that combining surface energy patterning with subsequent liquid metal printing methods could be a path forward towards additively patterned 2DMO printing.

2.4 Cabrera Mott Oxidation Model for Liquid Metal Interfaces

Surface oxides grow spontaneously on metals at low temperatures by Cabrera-Mott (CM) oxidation (**Figure 5a**), a model put forward in 1949 by N. Cabrera and N.F. Mott[60]. The CM model describes the formation of nanoscale surface oxides (Figure 2a) as a balance of metal cation migration through the oxide driven by an electric field appearing from the adsorption of O^{2-} ions at the surface. The built-in potential across the nanometer thick oxide resulting from the difference in chemical potentials on either side is substantial (~ 1 eV), resulting in an electric field on the order of 10 MV/cm. **Figure 5b** shows a band diagram illustrating the classic CM predictions specifically based on assumptions of a thermal equilibrium state and an oxide layer free of space charge. The built-in potential equal to the product of the electron charge and the Mott potential is labeled as the quantity $q \cdot V_{bb}$, which Ramirez, et al. have argued is also equivalent to the Gibbs free energy of an adsorbed gas molecule in its reduced state on the surface of a CM grown oxide[61]. *In-situ* atmospheric pressure synchrotron studies of the growth of aluminum oxide surface oxides have recently confirmed these central hypotheses of the CM model[61].

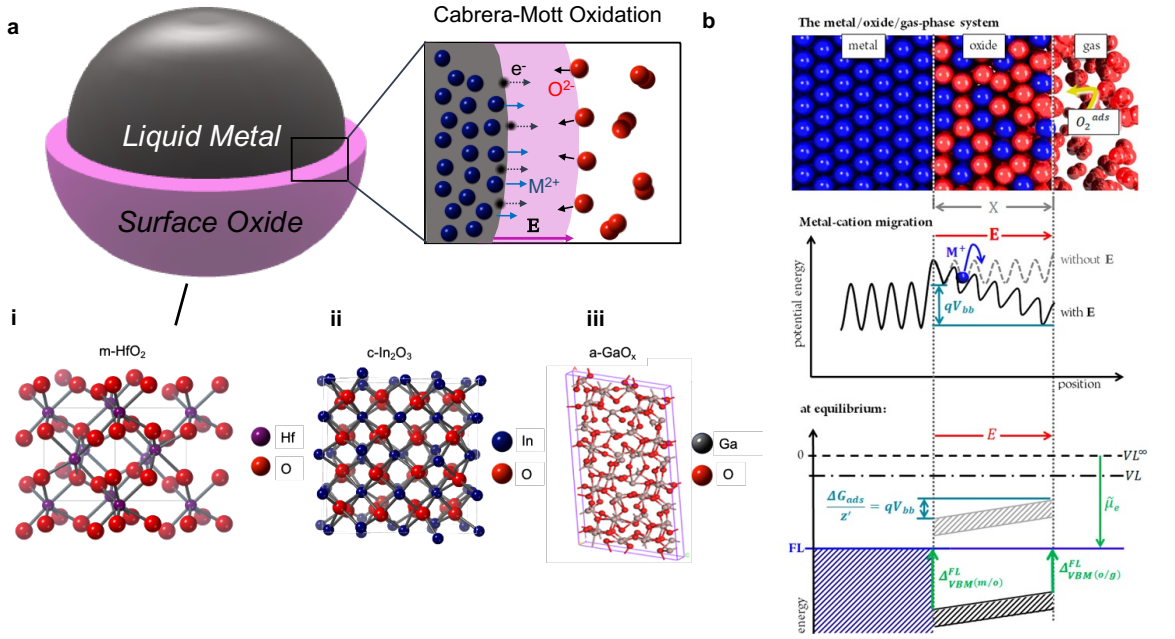

Figure 5*: (a) Schematic of Cabrera-Mott (CM) oxidation process forming solid metal surface oxides such as monoclinic HfO_2(i), cubic In_2O_3 (ii), and amorphous GaO_x (iii). (b)Diagram illustrating CM oxidation at metal / oxide / O_2 gas interface (top) illustrating mechanism for electric field assisted metal cation migration (middle) and the resulting equilibrium band diagram (bottom). Figure 5b reproduced from Ref.* [61].

Liquid metal printed 2D oxides have been primarily described by the physics of the Cabrera-Mott model. The majority of works reviewed herein have completed 2D oxide synthesis in highly oxidizing conditions (e.g. ambient air) over a range from room temperature to approximately 250 ˚C. Under these conditions, the solid 2D surface oxide is spontaneously formed *before*, or in many cases, *while* being transferred via Van der Waals forces to a target substrate. Removal of the excess liquid metal then allows the isolation of the 2D surface oxide. A central question since the beginning of this field has been how to predict the composition of the surface oxide for mixed metal precursor alloys, which may be required to maintain a low melting temperature. Several works in liquid metal synthesis of 2D oxides have put forward the hypothesis that the CM surface oxidation reaction for mixed liquid metals should be highly influenced by Gibb's free energy (tabulated for several common 2D oxides in **Figure 6a**). The assumption is that more thermodynamically favorable oxides should grow faster or displace less thermodynamically favorable ones. In the case of the liquid metal alloys reported by Zavabeti et al. in 2017[12], this theory can explain the predominance of HfO_2, Gd_2O_3, and Al_2O_3 over the oxides of Ga, In, and Sn in the quaternary precursor alloy. However, one limitation, as recently highlighted by Farrel et al.[38] is the fact that tabulated free energies are reported for stoichiometric crystalline oxides, which differ significantly from those formed in the highly non-equilibrium conditions of rapid CM

oxidation. This work suggests that instead of the free energy, the redox potential can be used to reliably predict the enrichment of alloy constituents in the surface oxide layer (**Figure 6b**).

The thermodynamics of this process are also critical for determining the thickness of the 2D oxides. **Figure 6c** summarizes the reported thickness for various liquid metal printed 2D oxides such as n-type Ga_2O_3 and In_2O_3 as well as p-type SnO[9,11] and β-TeO_2[10], which span from approximately 1 nm to nearly 4 nm for a single printed layer, as determined from AFM scans of step height (**Figure 6d**). 2DMO insulators such as HfO_2 and Al_2O_3 printed from higher melting temperature metals (Hf and Al) dissolved in solvent metal alloys such as Galinstan (i.e. In-Ga-Sn alloy) generally exhibit smaller thicknesses of 1 nm or less (**Figure 6e**). The thinner films of insulating 2DMOs are also consistent with the Mott's prediction of self-limiting growth as the electric field is reduced by the increasing thickness. Another interested trend that can be observed in this data is the influence of dopants such as Sn[62], Zn[63], and Sb[64] in 2D In_2O_3, which have consistently been reported to increase the thickness of the printed films by 20-30%. These dopants appear in the surface oxide at similar stoichiometry to that of the metal alloy despite the simple prediction that In_2O_3 should predominate based on its larger Gibbs free energy of formation. Goff, et al. have suggested that this could be due to the diffusion of these dopant metal atoms into the 2D oxides[65]. Further exploration of the control over doping in 2D oxides is essential for extending liquid metal printing to multicomponent alloys for synthesis of ternary and even quaternary oxides that may offer superior semiconducting characteristics and stability.

2.5 Crystallinity of Liquid metal-derived 2DMOs

One of the extraordinary properties of 2DMOs is the high degree of crystallinity that results from the low temperature interfacial synthesis process. This crystallinity is surprising given the ultrathin nature (< 2 nm) of 2DMOs, which is a factor that often leads to the amorphous phase for film growth by methods such as atomic layer deposition[66,67]. This follows from the thermodynamics of ultrathin oxide films, which predict a lower total of surface and interface energies for the amorphous compared with the crystalline phase[68].

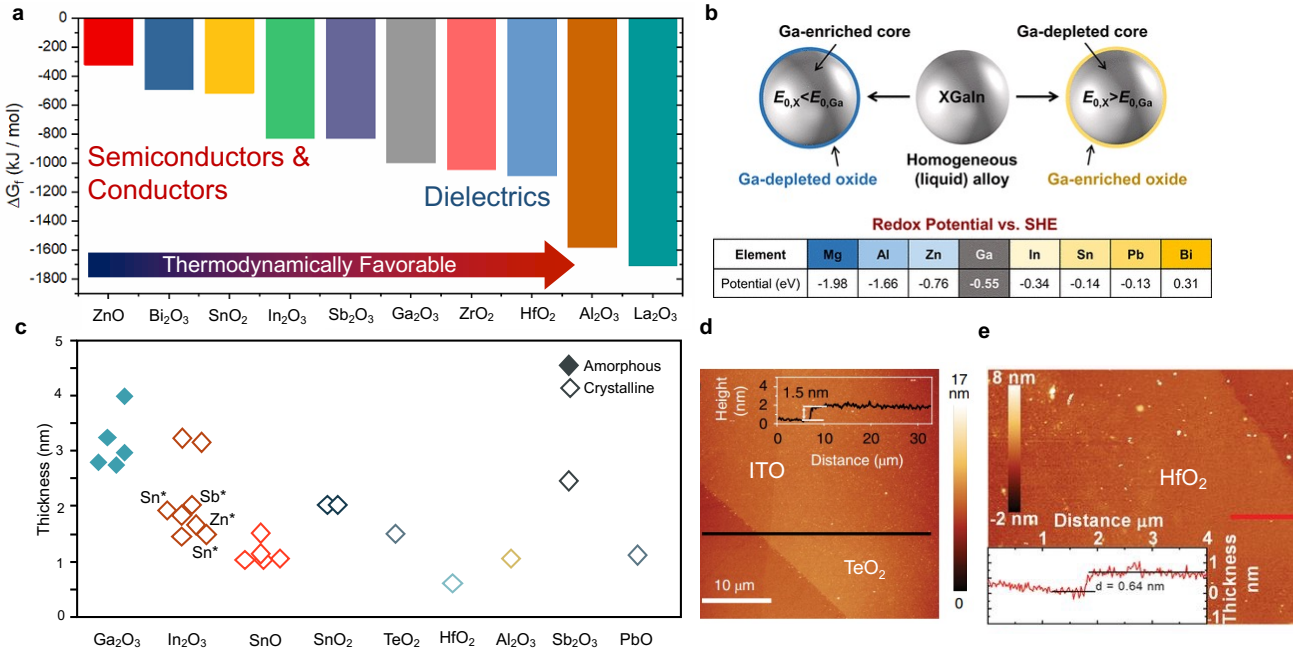

Figure 6*: (a) Gibbs free energy of metal oxides including semiconductors, conductors, and dielectrics. (b) Schematic illustrating reported surface enrichment of low redox potential elements on liquid metal alloys. (c) Summary of previously reported thickness for crystalline (closed symbols) and amorphous (open symbols) liquid metal printed 2DMOs. Atomic force microscopy (AFM) measurements of 2DMO layers of indium tin oxide (ITO) (d) reproduced from Ref.* [59] *and HfO_2 (e) reproduced from Ref.* [12]*. Part b reproduced from Ref.* [38]*.*

Previous studies of surface oxides of Al, Ni, Cu, Cr, etc. established a critical thickness of approximately 0.5 – 1 nm, depending on factors such as the oxide film strain, at which the transition to the crystalline phase is thermodynamically favored[69], however, we note that the kinetics of crystallization at low oxidation temperatures also tend to limit the observed crystallinity in most cases. We note here that the ability to repeatably synthesize oxide films at or near this critical thickness limit makes liquid metal synthesis a promising tool for fundamental material studies of ultrathin surface oxides. Despite the thermodynamic factors favoring amorphous films, 2DMOs just 0.5 – 3 nm in thickness tend to crystallize during their formation on the liquid metal surface[12], offering the potential to form large platelike grains (**Figure 7**) with lateral dimensions up to 10× greater than the thickness of the nanosheets. Under examination by HRTEM, these oxides such as In_2O_3 exhibit Moiré fringes indicating that their multilayers are indeed composed of independent crystallites stacked on top of each other. In semiconducting and conducting material systems such as In_2O_3:Sn (ITO) these vertically overlapped morphologies have potential benefits for improving electronic transport that may otherwise be limited by lateral grain boundaries[6]. The overlapped morphology could be thought of as analogous to basal plane aligned nanosheets of materials such as MoS_2, WS_2, and reduced graphene oxide (rGO)[70], for which the

vertical overlap provides efficient inter-sheet electronic transport. Magari et al. report[71] that high-quality sputtered polycrystalline In_2O_3 has electron mobility closely dependent on lateral grain boundary scattering for electron concentrations of 10^{19} cm^{-3} and below. This is one potential explanation for the considerable enhancement of the electron mobility observed for multilayers compared with single layers of semiconducting and conducting 2DMOs[2,6,7]. Datta et al. have also postulated that the lower measured Hall-effect mobility of single layers of ITO vs. double layers of 2D ITO could be due to the effective screening of interfacial defects by the initial layer[59].

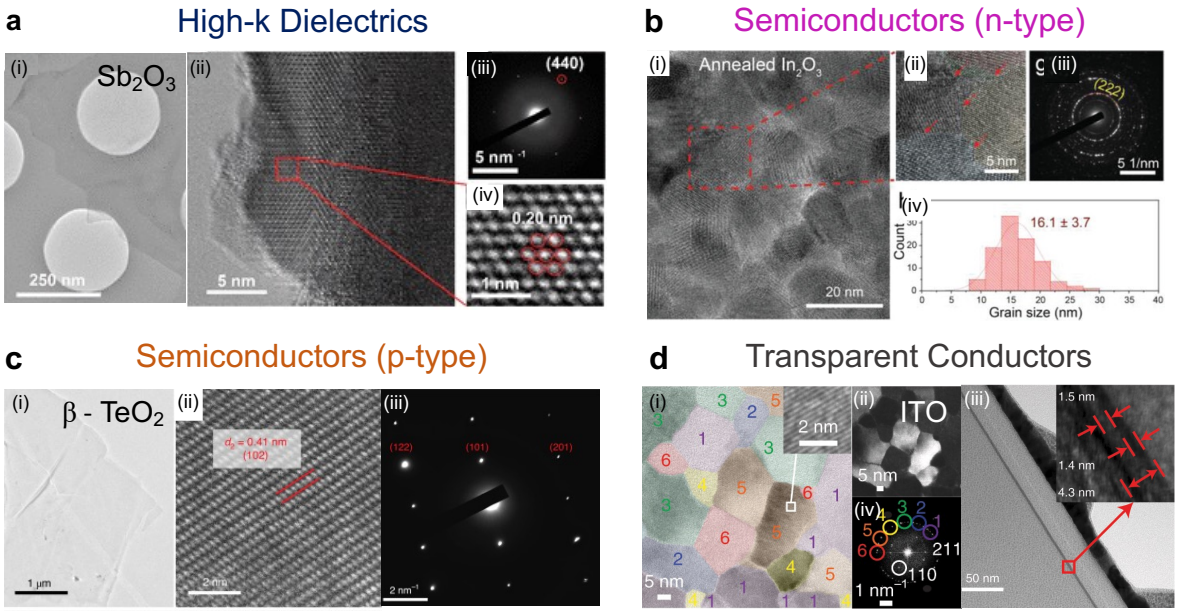

***Figure 7**: Summary showing TEM images of crystalline 2D liquid metal printed oxide materials including high-k dielectrics (a), n-type and p-type semiconductors (b,c), and transparent conductors (d). (Part a reproduced from Ref.*[16] *. Part b reproduced from Ref*[15]*. Part c reproduced from Ref*[72]*. Part d reproduced from Ref*[59]*.)*

The morphologies that result from large platelike grain growth in 2DMOs are also a distinguishing feature, since low-temperature crystallized cubic metal oxide films such as In_2O_3 typically result in grain sizes on the order of the film thickness[73]. Further studies in a recent report[15] by Nguyen and Daeneke have also shown that mixed 'heterophases' of amorphous-crystalline In_2O_3 can then be fully crystallized (**Figure 7**) by post-annealing, resulting in enlarged grains and high degrees of crystallinity favoring high mobility electronic transport. The degree of crystallinity of 2D surface oxides may depend critically on the kinetics of their formation. This is one factor which has been observed to generally impact crystallinity, for example, Zavabeti, et al. observed in 2017 that bubble-exfoliation synthesis yielded samples with low crystallinity while the same alloy produced crystalline samples via touch printing. The authors suggested that the rapid reaction at the liquid metal/bubble interface may have been responsible for the formation of the amorphous phase.

Bubble exfoliation synthesis of nanocrystalline tin oxide nanosheets has also been achieved, however, at temperatures[74] above 260 ºC to exceed the T_m of Sn. Recent work has also shown that post-annealing at up to 450 ºC can produce highly crystalline SnO_2 nanosheets that form 'fish scale-like' morphologies[75]. While semiconducting and conducting 2D oxides have benefitted from their high degree of crystallinity, there are specific application spaces such as that of high-k dielectrics which may call for engineering the formation of the amorphous phase. While high-k dielectrics such as Sb_2O_3[16] could offer higher capacitance in their crystalline phase (**Figure 7**), the high leakage associated with grain boundaries could present a challenge for achieving insulating gate dielectrics for applications to devices such as thin film transistors.

Amorphous Ga_2O_3 is an exception to the general trend of crystalline 2DMOs. Possible explanations for these reports of this glassy Ga_2O_3 phase could be the low melting temperature of Ga (T_m ~ 29.8˚ C) and its rapid formation rate[76], which could kinetically favor amorphous films. Ga_2O_3 deposition at 200 ˚C, for example, has been reported in one case to result in films in the crystalline β phase by Li, et al. in 2021[24] but amorphous films in nearly all other reports[13,77–79]. The formation of amorphous Ga_2O_3 on metallic Ga was previously thought to result from the ultrasmooth but disordered liquid Ga surface[80], although this rationale would not explain the formation of highly ordered, crystalline 2D oxides (Al_2O_3, HfO_2, Gd_2O_3, etc.) at the Galinstan interface in other prominent studies[12]. Control over the crystalline vs amorphous phase could be essential, however, for developing future device applications of 2D-Ga_2O_3 in emerging neuromorphic devices[78] utilizing its insulating vs conducting character. Wide bandgap beta-phase Ga_2O_3 is also widely accepted as promising for power electronics and ultra-violet sensing device applications. Some recent studies have shown the ability to crystallize liquid metal printed amorphous Ga_2O_3 via thermal annealing at 800 ºC[81].

2.6 Composition and growth kinetics of 2DMOs

The electronic and optoelectronic properties of 2D oxides depend critically on their chemical composition and thickness, both of which can be engineered from the liquid metal precursor. N-type multicomponent oxide semiconductor systems, in particular, offer a large space for material design to develop high-performance electronic devices. However, controlled doping of multicomponent metal precursor alloys to print ternary and quaternary oxides has proved more challenging than might be expected. Perhaps the most relevant well-studied case is the surface oxide of eutectic Gallium Indium (eGaIn) (75.5% Ga, 24.5% In), which preferentially oxidizes to form a surface layer of Ga_2O_3. Recent work by Thuo, et al.[82] has shown that this leads to the segregation of In to the core of eGaIn particles, as Ga_2O_3 builds a passivating oxide shell with minimal In_2O_3 content. These observations match the reports of Zavabeti, et al. in 2017 that alloys with more oxyphilic elements (e.g. Gd, Hf, Al) with large negative Gibbs free energies of oxidation

will have surface oxides dominated by those elements' surface oxides (e.g. Gd_2O_3, HfO_2, Al_2O_3) [12].

However, recent work has revealed alloys with elements such as Zn that should be displaced in the surface oxide, yet appear consistently, for example, lightly Zn-doped InO_x reported by Jannat, et al.[63] and Zn-doped Ga_2O_3 reported by Liu, et al[83]. Both of these alloys should exhibit little Zn content if the oxide composition was determined strictly by the free energy of formation. As noted by Farrell and Tabor in their recent work mentioned in Section 2.1, the redox potential of metals can predict surface enrichment (observed by X-ray photoemission spectroscopy (XPS)) of large negative redox potential metals such as Al and Mg dissolved in liquid metals such as Galinstan (68.5% Ga, 21.5% In, 10% Sn)[38]. An implication of these studies is that metals such as Zn should be capable of dominating the surface oxide in allows with In and Sn despite the less negative Gibbs free energy of formation of ZnO compared with In_2O_3 and SnO_2. Similarly, Ghasemian, et al. have demonstrated via molecular dynamics (MD) simulations how such surface enrichment of Sn-based liquid metal alloys with low percentages of Zr and Hf can lead to the formation of 2D SnO - $HfZrO_x$ nanosheets exhibiting ferroelectricity[84]. Recent MD studies have also shown that near-surface ordering of liquid metal atoms can influence the initial oxidation process of liquid metal alloys such as Galinstan (GaInSn)[85]. Additionally, a ternary $InZnSnO_x$ based on a liquid metal printed In-Zn-Sn alloy was recently demonstrated by Li, et al[14]. Though quantitative analysis of the film composition was not reported, the authors showed XPS and EDS evidence of the presence of relatively even percentages of Sn, Zn, and In in the resulting film printed at 200 ºC. Finally, another important consideration is the distribution of dopants or alloy constituents in 2D oxides.

Liquid metal printing of Sn-based alloys has also revealed the importance of surface segregation and oxidation rate. Recent work by Ghasemian and Kalantar-Zadeh has shown that Sn-Bi alloys exhibit a tendency for Sn to segregate to the surface but also accommodate the formation of Bi_2O_3 nanograins embedded in a larger polycrystalline SnO phase[39]. An additional recent report shows that beyond the total composition of the oxide film, the distribution of ZnO, In_2O_3, and Ga_2O_3 phases is not necessarily homogeneous, but instead can form a mixed crystalline and amorphous phase dominated by amorphous Ga_2O_3[86]. Recent work by Chen, et al. has shown a mixed phase in 2D oxides printed from In-Sn-Bi alloys consisting of crystalline domains of In_2O_3, Bi_2O_3, as well as SnO_2. The net result of this mixed phase was reported to be an increase in the conductivity of the ITO films as a result of the inclusion of the Bi_2O_3 phase[87].

Several recent studies have shown that the kinetics of metal surface oxidation can determine the resulting metal oxide film oxygen stoichiometry, for example, controlling the concentration of oxygen vacancies. A recent study by Atkin and Kalantar-Zadeh demonstrated that the early phases of oxidation of molten Sn result in SnO while longer oxidation produces thicker

multilayer SnO_2 films[52]. This suggests an important connection between the oxygen stoichiometry and the speed of oxidative 2DMO processing, with slower printing speeds favoring the formation of more oxygen-rich 2DMOs while high speed printing favors the formation of more oxygen-deficient films. Controlling this oxidation rate could be essential for determining the electronic properties of various metal oxides that depend closely on the concentration of defects such as oxygen vacancies. Though a detailed study of the growth kinetics of liquid metal printed 2DMOs has not yet been published, to our knowledge, there is recent evidence of logarithmic growth for In_2O_3 film as a function of increasing oxidation temperatures. Liao and Wu reported in 2023 that 8-12 nm layers of In_2O_3 can grow on a film of In at 400 ºC with increasing partial pressure of O_2[88]. In this paper, Liao and Wu model the growth of their indium oxide films using a logarithmic law (Equation 1) of the form suggested by Cabrera and Mott, with a film thickness L and time, t:

$$\frac{1}{L} = A - B \ln t \quad (1)$$

Liao et al. reported good agreement with the inverse logarithmic growth law, though we note that their growth took place at a considerably higher temperature than most reports of liquid metal printing. More detailed studies of the kinetics specifically of low temperature liquid metal oxidation have not been reported in this field, perhaps due to the difficulty of precisely controlling the kinetics of the process. Methods with a controllable deposition speed such as blading or CLMP could, in theory, provide an opportunity for thoroughly probing the kinetics of liquid metal surface oxide growth. We highlight this particular issue as it could help advance both the accuracy and the fundamental understanding of liquid metal printing.

3. Device Integration of Liquid Metal Printed 2DMOs

3.1 2DMO channels for Thin Film Transistors

2DMOs produced by liquid metal printing can be designed to offer high mobility and ideal semiconducting characteristics for electronic devices such as thin film transistors (TFTs) and diodes. N-type In_2O_3 and ITO are well-known materials for developing high-performance electronic devices because of their intrinsically high electron mobility (>100 cm^2/Vs) and wide bandgap nature over 3.0 eV. However, these materials have excess free carriers and are highly conductive. Therefore, devices based on highly conductive 2DMOs must first leverage their ultrathin nature (2-3 nm thick layers) to maintain a sheet carrier density suitable for effective gating with high I_{ON} / I_{OFF} ratio[6]. Nomura et al[51] have modeled how this limits the effective full charge depletion of channels of 2DMO semiconductors (e.g. ITO) to a specific range of thicknesses (e.g. < 3.4 nm) depending on their carrier concentration as well as the capacitance of the gate dielectric,

with higher capacitance high-k dielectrics producing excellent switching even for highly conductive channels. An interesting result of the combination of high-k dielectrics with 2DMO channels is also the shift in V_{on} towards enhancement mode operation, a requisite characteristic for most analog/digital circuit-level applications towards practical electronic applications. Recent studies of the band structure of 2D In_2O_3 via density functional theory (DFT)[89] have shown how ultrathin films below 2 nm initiate a substantial widening of the electronic bandgap due to the quantum confinement effect, which potentially further improves the device performances of 2D In_2O_3-based electronics. Interestingly, In_2O_3 has the unique ability to maintain efficient electronic transport even with ultrathin channels down to 0.7 nm, thinner than a single unit cell.

Post-annealing processes at relatively low temperatures (only 250 ˚C) can improve the crystallinity of 2DMOs, enlarging grains and enhancing electronic transport, leading to devices with state-of-the-art performance approaching a linear mobility of 100 cm^2/Vs[15] on par with the best vacuum-processed films of these materials. Post-annealing also allows the use of 2DMOs made up of double layers printed on top of each other, since the annealing process can control the free-carrier concentration and produce devices with steep turn-on (low subthreshold slope) and high $I_{on}/I_{off} > 10^7$[6], as shown in **Figure 8.** Doping techniques afford greater control of the electronic structure and the free carrier concentration of InO_x thin films to improve performance and reduce variability. Two persistent challenges for highly conductive In_2O_3-based channel materials derive from the presence of high-density oxygen vacancy defects, namely that pure In_2O_3 usually exhibits low bias-stress stability unsuitable for most circuit applications and that large negative gate voltages must be applied to achieve full depletion of the channel in many cases. Metal oxide semiconductors can be engineered to remedy these defects by introducing elements such as Ga, Al, etc. that tightly bind oxygen due to their higher enthalpy of formation, reducing free carrier concentrations[90] and stabilizing these channels during bias-stress[91].

Table 3: Summary of performance and channel thickness of reports of liquid metal printed thin film transistors. (*thickness of double layer channels) **(exhibits significant contact barrier)

Reference	Channel	p vs. n type	Mobility (cm^2/Vs)	I_{on}/I_{off}	Thickness (nm)
[15]	In_2O_3	n	96± 4.8	10^4	1.9
[6]	In_2O_3	n	67	10^7	1.9 (4.8)*
[62]	ITO	n	23.2	10^9	1.9
[92]	ITO	n	27	10^9	1.9
[28]	GaS	n	0.2	10^2	1.5

[9]	In_2O_3/SnO	n	37	< 10	5.5
[93]	InO_xS	n	20.4	60	2.4
[64]	Sb doped In_2O_3	n	39.4	10^4	1.9
[63]	Zn-doped In_2O_3	n	87	10^5-10^6	1.6
[20]	InO_x/GaO_x Bilayer	n	22.6	10^6-10^7	3.2/3.0
[94]	$InGaZnO_x$	n	14.3	103	2.7 (5.4)*
[14]	$InZnSnO_x$	n	0.37	10^6	5
[11]	SnO	p	0.47	10^6	1.0
[95]	β-Ga_2O_3	p	21.3**	10^4	4-8
[10]	β -TeO_2	p	146 ± 42**	10^5	1.5
[96]	Ga_2S_3	p	3.5	10^2	2.0

Doping using cation dopants also offers the potential to enhance the mobility of 2D oxide semiconductors by the formation of hybrid orbitals and can be used to control the free carrier concentration beyond the limits of intrinsic binary oxides. C.K Nguyen showed that antimony doping introduced in the liquid metal precursor can enhance pure In_2O_3 printed at 250 ˚C to an electron mobility of 39 cm^2/Vs[64], albeit, with a corresponding increase in the off-state leakage current compared with that of other reports of pure 2D In_2O_3 at 250 ºC[6]. Similarly, Jannat et al. reported Zn-doped liquid metal printed 1.6 nm thick 2D In_2O_3 channels with increased

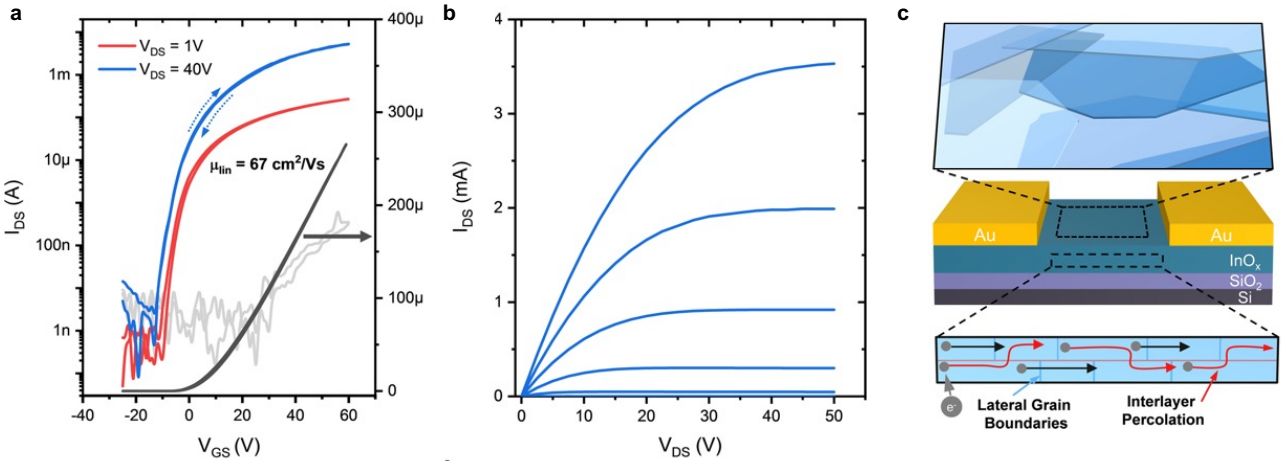

Figure 8: *Transfer characteristics (a) and output characteristics (b) for liquid metal printed In_2O_3 thin film transistor printed at 160 ºC. (c) TFT device architecture and proposed mechanism for overlapping bilayer platelike grain morphology with efficient inter-grain transport. Reproduced from Ref.*[6].

conductivity and determined a field effect mobility of 87 cm^2/Vs, though this work does present some non-linearity in low-drain field characteristics suggesting a potential contact barrier. By contrast, Sn-doped 2D In_2O_3 channels demonstrated by Nomura et al.[62] exhibit a reduction in the free carrier concentration and a control over the turn-on voltage in response to higher amounts of Sn-doping (10%), yielding low-off current and I_{on}/I_{off} of greater than 10^9. Representative transfer curves for these ITO transistors are provided in **Figure 9**, which depicts performance as a function of Sn doping and annealing temperature as well as demonstrating the steep switching achievable by pairing these 2DMO channels with high-k dielectrics. Incorporation of both Ga and Zn into an indium precursor alloy was recently demonstrated by Du, et al., showing $InGaZnO_x$ channels with approximately a 3-6-1 ratio of Ga-In-Zn in the oxide film[94]. In this work, the authors report a turn-on voltage near 0 V and a linear mobility of approximately 14 cm^2/Vs. Interestingly, the channel materials examined by electron microscopy revealed crystalline domains of ZnO and In_2O_3 embedded in an amorphous Ga_2O_3 matrix.

As a friendly reminder regarding 2DMO transistor measurements to propel this field toward technological maturity, we also note the best practices[97] established in related academic communities such as organic thin film transistors (OTFTs) that maintain that the linearity of measured transfer characteristics (which can be distorted by severe hysteresis and contact effects) is essential for accurately determining the effective carrier mobility. Contact effects as well as current spreading from un-patterned semiconductor layers are both sources of significant error that could cloud comparisons of 2DMO semiconductors. The measurement and presentation of linear scale transfer characteristics, full double sweeps, as well as full output curves are steps in the right direction in this regard. These best practices also serve to advance 2DMOs towards large scale applications (e.g. displays) requiring near ideal FET performance and low variability.

We note that this broadly reported finding of improved mobility of 2DMOs after doping

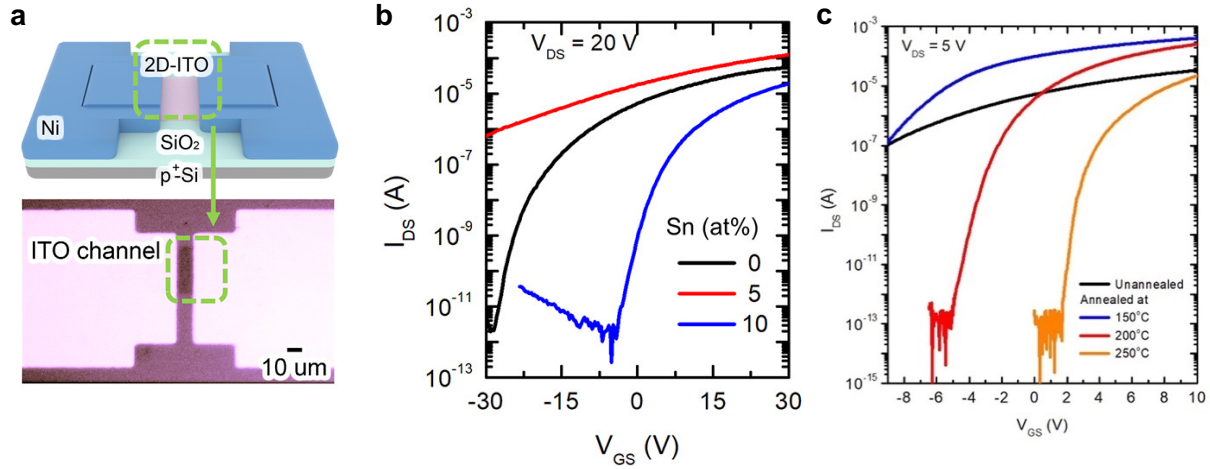

***Figure 9**: (a) Thin film transistor device schematic and microscope image with 2D-ITO channel. (b) Transfer characteristics of 2D ITO channels with varying doping concentrations. (c) Transfer*

characteristics of low operating voltage 2D ITO transistors with high-k Al_2O_3 dielectrics following post annealing in air at various temperatures (150 – 250 ºC). Parts a-c reproduced from Ref. [51].

runs counter to the conventional theories governing electronic transport in ordered, single-crystal semiconductors, in which ionized dopants introduce additional scattering centers and structural disorder at high concentrations. Metal oxides, as disordered materials with a high concentration of electron traps, have different dominant scattering mechanisms than single crystal semiconductors, depending to a greater extent on trapped carrier scattering and phonon scattering[98]. One result is that metal oxide channel materials may be particularly sensitive to the positive effects of gate-induced high density free electron screening, which can mitigate the impact of trapped carrier scattering[99] to enhance the mobility in the on-state. One explanation for the extremely high field effect mobility reported for 2DMO channels can be considered their high carrier density for maximizing the benefits of carrier screening.

Electrostatic design of 2DMO channels calls for balancing the free high carrier concentration of these materials by scaling down the channel thickness (**Figure 10a**). In recent work[11], Nomura et al. summarized this electrostatic design condition specifically for 2DMOs in the form of **Figure 10b**, plotting the limits for full depletion of a 2DMO channel (e.g. p-type SnO). For a given dielectric material (e.g. SiO_2 or Al_2O_3) with a specific permittivity and breakdown field (E_{BR}), an operating voltage can be chosen to remain within limits suitable for long-term operation, imposing a 'gate-induced charge limit' on carrier concentration or the channel (as a function of thickness). For ultrathin 2DMO channels, for example, just 1-3 nm thick, this plot defines a range of carrier concentrations (up to 3×10^{19} cm^{-3} for 3 nm channels, up to 10^{20} cm^{-3} for 1 nm channels) for which full depletion can be achieved. A consequence of these calculations is that full depletion and low off-state current can be achieved even for channel materials such as In_2O_3[6] and In_2O_3:Sn[51] with high free carrier concentrations ($n_0 \sim 10^{19}$ cm^{-3}) so long as the full depletion limit is satisfied. For additional background and analytical expressions of the electrostatic modelling of metal oxide thin film transistor channels, the authors recommend a concise but thorough treatment of the subject by Wager[100]. One conclusion from this work is that optimal metal oxide TFT performance favors channels thinner than ~ 2X the Debye length in the semiconductor, providing a guideline applicable to many different 2DMOs.

Figure 10c illustrates a plot of the mobility of these doped n-type 2D oxide TFT as well as those of pure In_2O_3, Ga_2O_3, and heterostructures of In_2O_3, SnO, and GaO_x. The symbol color in **Figure 10c** is mapped to the thickness of these channels, the majority of which have been reported at less than 2 nm. These recent works in the field of n-type 2D oxide semiconductors have reports a linear, low-field mobility beyond 20 cm^2/Vs, a mark that places them alongside some of the highest performing printed metal oxides reported to date for sol-gels and nanoparticles fabricated

at processing temperatures less than 250 ºC[101]. However, for applications to display technology, a primary technology for metal oxide semiconductor devices, the mobility is but only one performance metric. In reality, 2D metal oxide transistors must achieve low off-current, high switching ratios, and robust bias-stress characteristics before they can be integrated into larger scale, high performance circuits for large area electronics. Use of industrially relevant contact materials such as ITO, W, or Mo would support long-term goals of circuit integration and would facilitate additional studies of specific contact resistance that will be important to determine performance for < 5 μm channel length devices relevant to modern display technologies.

A main driver of the adoption of amorphous metal oxides in the display industry has been their ability to offer low leakage (off-current) for reducing static power dissipation compared with LTPS technologies[102]. In this regard, most reported 2D oxide transistors have not yet achieved commercially relevant levels of off-current, low hysteresis, and competitive bias-stress stability, though passivation layers based on coatings such as atomic layer deposition (ALD) coated Al_2O_3 can significantly improve these operational stability characteristics[51]. In one of our recent studies, we have reported the potential for liquid metal printed 2D Ga_2O_3 to serve as a passivation layer for improving off-state characteristics and limiting variability in 2D In_2O_3 TFTs[20]. Another recent report has shown that this passivation effect of ultrathin Ga_2O_3 can extend to other high performing 2D semiconductors such as graphene, suppressing interfacial phonon scattering[103]. Similarly, Zhang, et al. showed in 2023 that liquid metal printed Ga_2O_3 can passivate the interface of WS_2 to improve the growth of high-k dielectrics on TMDC materials[104].

Liquid metal printing has also provided a promising platform for processing hole-conducting semiconductors such as SnO for p-channel transistor development, which is required for complementary MOS circuits. For example, Nomura et al. demonstrated in 2021 (**Figure 10d**) that ultrathin liquid metal printed p-type SnO from pure Sn precursors could achieve a hole mobility of 0.5 cm^2/Vs and steep turn-on at thicknesses of just 1 nm[11] by utilizing ALD Al_2O_3 passivation and subsequent hydrogenation. These results are plotted in **Figure 10e**. This demonstration also combined liquid metal printed complementary devices from p-type SnO and n-type In_2O_3 to form inverters with a high voltage gain of 117 V/V. Recently, Zavabeti, et al. have reported a 1.5 nm thick p-type β-TeO_2 with a field effect extracted hole mobility of 146 ± 42 cm^2/Vs and a Hall-effect mobility of 141 cm^2/Vs, though we note that the transistor output curves exhibit a significant injection barrier at low drain voltages that could impact the extraction of the mobility. This remarkable performance of β-TeO_2 exceeds the mobility of other p-type metal oxides such as NiO_x (~ 4 cm^2/Vs[105]) and CuO_x (~12 cm^2/Vs[106]) by an order of magnitude, and offers significant advancement for p-channel TFT development. We note, however, that Tellurium as well as the Selenium alloys used for printing 2D β-TeO_2 bear considerable environmental[107] and health risks[108].

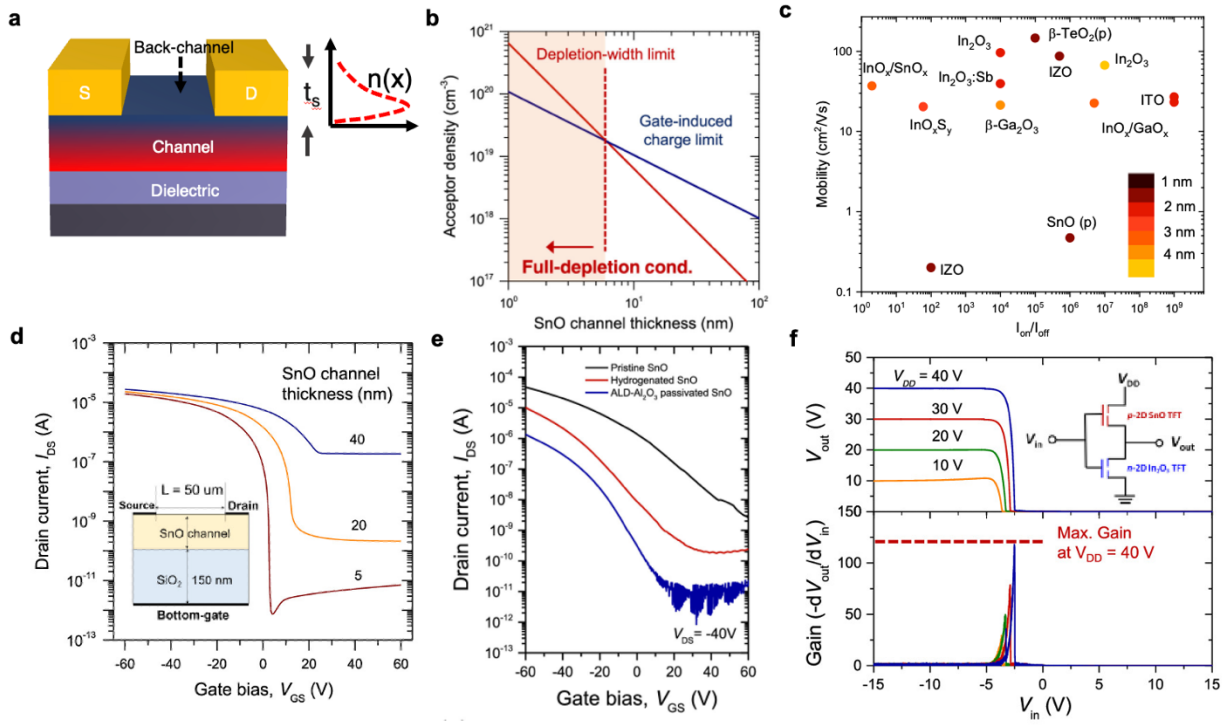

Figure 10: *(a) Summary of reported linear mobility of 2D oxide thin film transistors plotted as a function of the I_{On}/I_{Off} ratio. Symbol color maps to color bar of channel thickness. (b) schematic of 2DMO thin film transistor indicating back channel and distribution of accumulation layer charge relative to depth (x) in the channel. (c) Mapping of the limit of full depletion for 2DMO channels as a function of the acceptor density for a SnO channel vs. thickness.*[109] *(d) Transfer characteristics simulated for SnO TFTs of thickness 5 nm, 20 nm, and 40 nm. (e) Transfer characteristics of SnO p-type TFTs annealed with hydrogen and passivated with ALD deposited Al_2O_3 layers. (f) Inverter output signal as a function of input with lower plot showing gain vs. Vin for inverter composed of 2D oxide NFET and PFET (as shown in the inset). Figures 9c-f are reproduced with permission from Reference* [109].

Heterostructures of 2DMO can also provide a basis for engineering electronic transport through modulation doping, a strategy which uses the conduction band offset at the heterointerface to enhance the free carrier concentration. This conduction band offset can be produced, for example, at the interface between In_2O_3 and wider gap Ga_2O_3, inducing a degenerate electron concentration without introducing structural disorder or compensation effects from extrinsic dopants. In our recent work, we applied this approach to fabricate superlattice multilayer In_2O_3 / Ga_2O_3 films at high speeds and low temperatures (180 ºC), with higher performance (conductivity > 600 S/cm) than competing printed transparent conductive oxide electrode materials[7].

3.2 Optoelectronic Device Applications of 2DMOs

2DMOs offer several useful properties that can facilitate their integration into optoelectronic devices for high sensitivity photodetection of ultraviolet (UV) and visible light as well as photonic circuit applications. A number of recent works have applied liquid metal synthesized 2D oxides

for photodetection. The high visible range transmittance of 2DMOs (> 99%), firstly, supports their use as transparent electrodes but also their use as the active component of visible blind detectors with optical bandgaps > 3eV. These applications allow 2DMO optoelectronics to harness the same advantages of large area deposition, low temperature fabrication *and the ability* to make these systems mechanically flexible via integration on polymer substrates. The goal of photodetector integration is to achieve a high responsivity (current per incident optical power) with low dark current and a good degree of selectivity to the desired wavelength.

UV photodetection has been achieved with 2DMOs down to 2 nm thick. For example, Sb-doped In_2O_3 was recently shown, in a lateral substrate-gated transistor geometry, to exhibit a photoresponsivity of above 1000 A W^{-1} for 285 nm photons, though these devices showed a long recovery time (> 2000 s) due to the influence of the persistent photoconductivity of In_2O_3[64]. Similarly, $InZnSnO_x$-based TFTs exhibit a strong photo-response to UV excitation, albeit with longer than ideal response times of 6 – 37 s[14]. Vertical photodetector architectures incorporating 2D Ga_2O_3 printed from liquid metals with Si have shown visible-blind photodetection of 254 nm and 365 nm light with slightly lower responsivity (40-50 A W^{-1}) but with a significantly faster response (rise time 0.2 ms and fall time 2 ms)[24]. In this case, the wide bandgap (4.8 eV) of 2D Ga_2O_3 provides for the selective response to deep ultraviolet excitation. The bandgap of Ga_2O_3 can be decreased through alloying with lower bandgap oxides such as Bi_2O_3 through liquid metal printing of Bi-Ga alloys, as shown in a recent paper by Huang et al[110]. In addition to demonstrating a lateral photodetector with 959 mA W^{-1} responsibility, the authors show ultraviolet photoelectron spectroscopy measurements indicating a significant shift in the work function of the liquid metal printed Ga_2O_3 films upon introduction of 5-15% of Bi in the precursor alloy.

Visible range photodetection can be achieved through chemical transformation of 2D oxides into other families of 2D materials. Methods such as sulfurization of 2D Ga_2O_3 to Ga_2S_3 can lower the optical bandgap to approximately 2.1 eV, providing for a strong response to visible light (240 A/W)[96] in films just 2 nm thick. Even partial sulfurization of In_2O_3 to form InO_xS_y can also lower the bandgap and provide benefits for photodetection, yielding a high responsivity of 3400 A/W[93]. Tin based liquid metal printing can allow synthesis of visible and even longer wavelength absorbers. Liquid metal printed SnS films have provided a way to extend the photoresponse into the visible range (**Figure 11a**) as well as the near infrared (NIR), with a measured bandgap energy of 1.41 – 1.80 eV that depends on the thickness of the stack of 2D SnS layers[111]. Photodetector devices based on SnS exhibit responsivity of approximately 1000 A W^{-1} for 660 nm excitation in a lateral architecture, with an impressively fast response time of 20 – 50 μs. Stacks of 2D oxides can be used to form metal oxide-based p-n junctions for allowing unique sensing functionality. For example, Alsaif et al. demonstrated the fabrication of a 2D SnO/In_2O_3 heterostructure formed by overlaid liquid metal printing steps, yielding photodetectors with high

detectivity and photoresponsivity (1047 A W^{-1}) in the UV range based on the p-n diode structure[9]. Interestingly, devices exhibited higher sensitivity to illumination at 280 nm compared with non-heterostructure devices composed of only In_2O_3 or only SnO.

Collectively, these various demonstrations of photodetections illustrate an opportunity for utilizing the scalability of 2DMO processing to afford high uniformity and the capability for large area integration of arrays. One potential application of these 2DMO based photodetector devices, due to their potential for integration with display backplanes, is towards in-pixel sensing. In this application, pixel-integrated photodetectors can provide sensing capability for finger print detection and biometric analysis[112]. Another avenue for both boosting performance and achieving deeper integration with technologies such as displays is to utilize phototransistor architectures[113] that amplify sensitivity with photoconductive gain. With their high transparency and excellent electrostatics, 2D oxides could offer an ideal platform for efficiently collecting photocarriers generated by other highly absorbing materials in the visible or infrared spectrum. Finally, we note an emerging direction for 2DMOs which is in devices that can leverage their non-linear optical behavior demonstrated by Zhang et al. in 2024[114]. Zhang et al. show a large second-order susceptibility (χ^2 of ~1,800 pm V^{-1}) by using the quantized effect of liquid metal printed 2D ITO, which is more than 20 times higher than that of the traditional nonlinear $LiNbO_3$ crystal. These results indicate that 2DMOs can be harnessed for future nonlinear photonic circuit applications. The potential for heterostructure formation and complex 2DMO stacking could facilitate these new directions.

3.3 Emerging Device Applications of 2DMOs – Sensing, Neuromorphic Computing, and Energy Harvesting

Recent works have applied 2DMOs towards neuromorphic computing applications, demonstrating the potential benefits of their ultrathin nature. For example, liquid metal printed 2D Ga_2O_3, can offer *forming-free* non-volatile resistive switching[78] taking advantage of the ultrathin amorphous structure. The device stack consisting of Pt electrodes on 2D Ga_2O_3 on Si showed a retention time greater than 10^4 s, a contrast of approximately 300X between the low resistance (LRS) and high resistance state (HRS), and demonstrated multilevel resistive switching for synaptic potentiation and depression[78] (**Figure 11c**). The memristive behavior of vertical device architectures based on Ga_2O_3 have also been recently explored by Akbari et al[115], who recently demonstrated GaS doped Ga_2O_3 fabricated through a plasma based process (H_2S plasma). By directly electrically measuring oxidized eGaIn droplets with a conductive AFM tip, this work showed high contrast between LRS and HRS states even within an operating window of less than ± 1.0 V. Liquid metal printed 2D InO_x has substantially higher conductivity than Ga_2O_3, but it also

recently been integrated into memristor device architectures by Huang et al[116]. In this work, the authors use a 2 μm lateral channel with Ti/Au electrodes formed by printing 2 – 5 nm layers of InO_x at 180 ºC. The authors observe approximately 10-50X contrast in the LRS vs. HRS resistance values and demonstrate the ability to modulate the memristive state with short or long duration write voltage pulses, leading to mimicry of Ca^{2+} dynamics in neurons. One interesting observation from this study was that higher temperature printed InO_x, for example, films deposited at 200 ºC, did not display memristive behavior, suggesting that the microstructure and trap density in InO_x are critical for memristive behavior.

2D oxides can also be applied in three-terminal device architectures to precisely control memristive behavior. For example, Huang and Nomura have demonstrated dynamic analog switching using 2.5 nm thick 2D SnO_2 channel based memtransistors processed from molten Sn with a maximum process temperature of 250 ºC[117]. The three-terminal structure of these memtransistors allowed analog tuning of the value of the LRS and HRS by up to 100X using the applied gate voltage. This study showed the repeatable potentiation and depression with pulsed operation and simulated the performance in a typical neuromorphic computing application such as pattern recognition from handwritten digit image sets. Another recent study applied 2DMOs based on Sb-doped In_2O_3 for neuromorphic computation using UV light (λ =285 nm) as the stimulus for long-term potentiation[118]. This light tunable synaptic behavior leveraged the well-known persistent photoconductivity effect that has been problematic for engineering low bias stress response for oxide transistors in display technology[119]. Similarly, Ahmed et al. showed that 2D In_2S_3 formed via sulfurization of liquid metal printed 2D In_2O_3 can exhibit persistent photoconductivity and provide a material platform for demonstrating synaptic plasticity and synaptic learning[120]. A similar recent study has shown that liquid metal printed 2D In_2O_3 can also be applied for this purpose, demonstrating sensitivity to potentiation with visible range light (e.g. 455 nm)[121]. This result shows that the optical absorption caused by midgap defects can contribute to a significant persistent photoconductivity effect in two-dimensional oxides, a potential barrier to stability in certain optoelectronic device applications. While these demonstrations of neuromorphic computing using 2D oxides offer another potential application space, they serve as a reminder that the substoichiometry of 2DMOs can render them sensitive to bias stress and illumination, two factors that must be overcome before applying them towards most conventional circuit applications.

The ultrathin nature of 2DMOs such as In_2O_3 also makes them electrostatically ideal materials for sensing the concentration of various gas species. The design of semiconducting gas sensors with a thickness near or below the Debye length has advantages for promoting greater sensitivity via chemiresistive sensing mechanisms[122]. It is no coincidence that this design guideline for sensors aligns well with the goal of making ultrathin 2DMO semiconducting channels

in thin film transistors. By enhancing sensitivity, 2DMO layers also provide an opportunity for minimizing the need for additional heaters that otherwise drastically increase the power consumption of traditional gas sensors. Cheng et al., have shown that single-layer crystalline 2D In_2O_3 films with thickness near 2 nm provide larger relative responses (changes in conductivity) to gas species such as NO_2[123]. Furthermore, the work by Guo and Zavabeti, et al. has shown single ppm-level sensitivity of liquid metal printed 2D In_2O_3 to gases such as NO_2, NH_3, and CO with relatively fast (~ 20 – 70 s) response times[3]. Though these 2D oxide gas sensors were operated at elevated temperatures of 200 ºC to improve sensitivity, field-effect architectures[124] and heterostructures[125] could offer the potential to enable room temperature gas sensing. Recent work by Nguyen, et al. has also shown the ability to use liquid

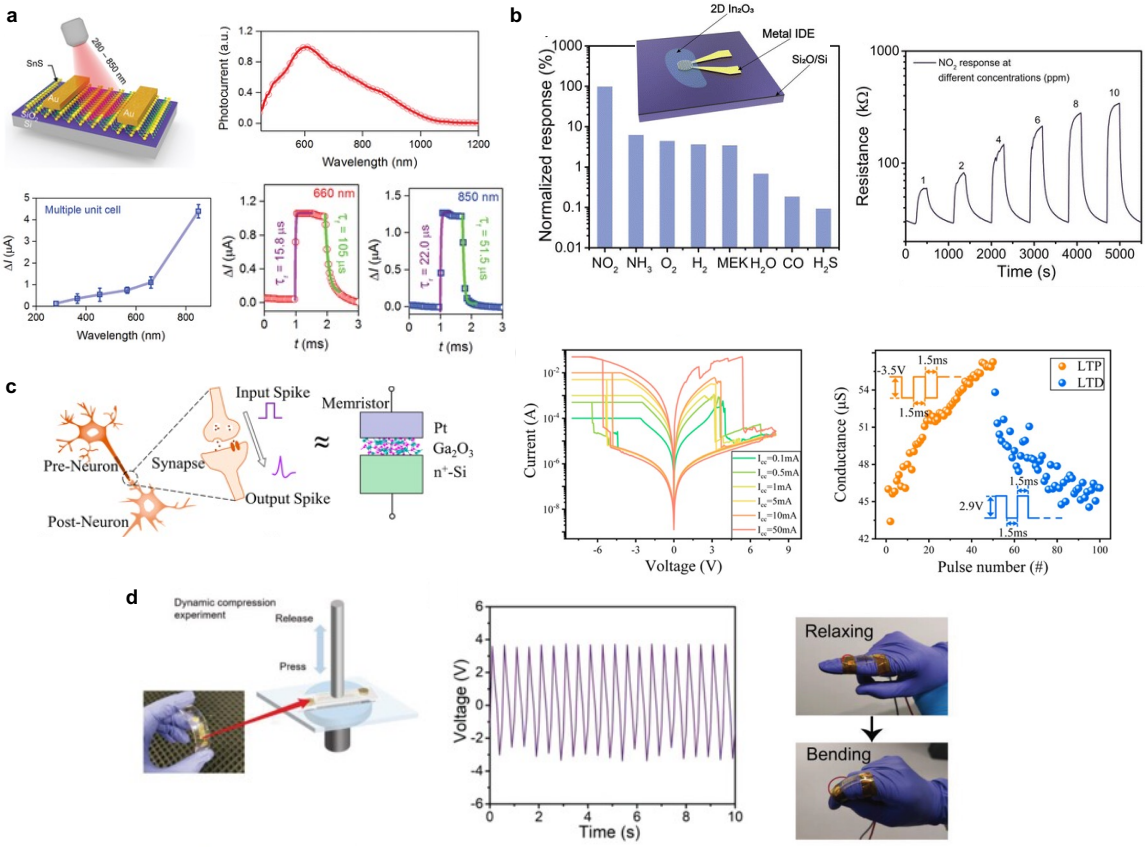

***Figure 11**: (a) Summary of 2DMO device applications including photodetectors and gas sensors. (a) NIR photodetectors based on 2D SnS synthesized from liquid Sn alloys. (reproduced from Ref. [111]). (b) Gas sensors based on liquid metal printed 2D In_2O_3 (reproduced with permission from Ref. [3]. (c) Application of 2D Ga_2O_3 vertical memristors to neuromorphic computing. [reproduced from Ref. [78]). (d) BiO_x piezoelectric oxide deposited on flexible substrate for energy harvesting. (reproduced from Ref. [56]).*

metal printed 2D SnO_2 in gas sensors at relatively low operating temperatures (150 ºC) to sense NH3 gas with high selectivity[126]. Work by Alsaif, Ou, and Zavabeti showed that 2-nm-thick films

of Ga_2S_3 printed from liquid Ga could also provide near room temperature (50 ºC – 150 ºC) detection of NO_2 gas (**Figure 11b**) at 10 ppm levels[96], with a minimal response time of 180 – 200 s. Oxychalcogenides such as $GaSeO_x$ can also provide a platform based on liquid exfoliated nanosheets to perform gas sensing, by Chen et al. showing an improvement in selectivity of the electrical response to NO_2(g) as compared with other species such as NH_3, SO_2, etc[127]. This work also In recent work, nanostructured BiTe synthesized from liquid metals was also shown to provide sub 1 ppm sensitivity to NO_2 gas at low operating temperatures[128]. The high surface area of these nanocrystals harvested from the eGaIn surface provided for greater sensitivity and effective charge transfer.

Similar to many other inorganic gas-sensing nanomaterials, 2DMOs and 2DMO-derived materials can exhibit a broad response to multiple gas species[3] without offering a sufficiently high degree of selectivity for certain sensing applications. Further studies characterizing cross-sensitivity to fluctuations in humidity, temperature, and other environmental characteristics will be essential for producing 2DMO-based sensors with industrially relevant capabilities. Integration of additional sensing layers on the surface of 2DMOs could enhance performance towards the ppb range of sensitivity[129]. Additionally, the integration of UV stimulation with gas-sensing could provide one potential strategy to accomplish room-temperature sensitivity[130].

Energy harvesting has emerged as a new application domain for 2DMOs. These nanogenerator devices apply the ability of liquid metal synthesis to produce crystalline, high quality piezoelectric oxides. For example, 2D films of metastable β-PbO grown on the surface of molten Pb were demonstrated by Ghasemian, et al. in 2020[4] to exhibit high vertical piezoelectric coefficients (30 pm V^{-1}) for films as thin as 1 nm. The authors argue for the utility of these ultrathin PbO films for reducing the total Pb content in piezoelectric sensors and actuators. Guo, et al. have reported[56] nanogenerators based on 2-3 nm thick piezoelectric α-$Bi_2O_{3-\delta}$ synthesized by transferring solid oxide nanosheets from the surface of liquid bismuth droplets. This study also reveals via density functional theory (DFT) studies that the substoichiometric liquid metal printed films of bismuth oxide containing high concentrations of oxygen vacancies can exhibit a strong piezoelectric response (**Figure 11d**) even though the centrosymmetric structure would not normally exhibit piezoelectricity. Another potential advantage of liquid metal printing these materials is that the piezoelectric coefficients in 2DMOs can also exceed the values for bulk crystals of the same composition. For example, a liquid metal synthesized 2D $GaPO_4$ reported by Syed et al.[18], in 2018 revealed a significant enhancement in the *d33* value compared with those reported in the literature for bulk $GaPO_4$. This effect of increased piezoelectric coefficients has also been reported by Khan et al. for 2D SnS formed on liquid metal Sn[131], producing efficient nanogenerators on flexible substrates. These performance advantages of 2D piezoelectric materials stand in addition to this capability also demonstrated by Guo et al. to transfer the piezoelectric oxides onto

stretchable substrates that can be applied for energy harvesting or electromechanical sensing in a variety of different applications that benefit from conformal or flexible form factors.

3.4 Synthetic Opportunities, Challenges, and Future Outlook for 2D Oxide Electronics

2DMOs have outstanding promise as a material system for flexible inorganic electronics and optoelectronics. The vacuum-free and solvent-free printing process is unique in its chemical simplicity and its thermodynamic advantages. In many features, including crystallinity and conductivity, 2D oxides are vastly different from solution-processed films[25] because of the physics of Cabrera-Mott oxidation, making 2DMOs electronic features resemble vacuum-processed films more than traditional printed semiconductors rich in defects. The surprising advantage is that 2DMOs constitute a large area printing technology when applying methods such as continuous liquid metal printing (CLMP)[13] that deliver high speed and scalability to large substrates. The large continuous films possible with this technology are unlike ultrathin materials produced from solution-processed 2D materials because they do not rely on percolation networks of 2D microscale flakes. This juxtaposition with 2D materials such as transition dichalcogenides (TMDs) has become timely as the 2DMO field has demonstrated the ability to convert 2D oxides into high-quality 2D selenides, sulfides, and nitrides.

Conversion of liquid metal printed 2DMOs to high performance 2D nitrides, selenides, and sulfides delivers the benefits of the large area deposition and low process temperatures. For example, the conversion of 2DMOs to nitrides has been accomplished via gas phase ammonolysis (**Figure 12a**) using urea as a source of NH_3 (g), yielding polycrystalline 1.3 nm GaN nanosheets at 800 ºC and 2 nm InN at 630 ºC[132]. These 2D III-nitride nanosheets exhibited quantum confinement effects resulting in slightly enlarged bandgaps (3.5 eV for 2D GaN). Hall-effect measurements indicated an electron mobility of approximately 21.5 cm^2/Vs for the GaN nanosheets. Recent work expanded on this method by utilizing N_2 plasma to convert Ga_2O_3 to GaN at low temperatures[95]. These GaN films were integrated into TFTs that demonstrated p-type behavior with steep subthreshold slope, albeit with superlinear output characteristics indicating a contact barrier to the Ag electrodes utilized in this study. This report is in contrast with similar liquid metal-derived GaN that adopts n-type characteristics[132,133] as determined by Hall-effect measurements. Interestingly, liquid Ga surfaces have also been applied in one recent work for CVD-based synthesis of single crystal GaN nanosheets with lateral sizes up to 50 μm, based on a urea-derived ammonia process at 1080 ºC, demonstrating 4-6 nm thick nanosheets with electron mobility above 160 cm^2/Vs. The potential for direct single-crystal synthesis on liquid metals points to opportunities for depositing large area films of high performance III-N materials. Other recent works, for example, by Pedram, et al.[134] has shown microwave-assisted plasma synthesis using N_2/H_2 plasma can perform a conversion of liquid metal printed Ga_2O_3 to GaN at a lower

temperature of 320 ºC, resulting in films with optoelectronic properties similar to those of bulk GaN. Li et al. have also recently shown the synthesis of 2D GaN using a plasma-assisted approach to lower the synthesis temperature to near room temperature, as shown in **Figure 12b**[95]. The potential for low temperature synthesis could afford additional back end of line (BEOL) integration with CMOS integrated circuits or, if further thermal budget reduction can be achieved, with flexible substrates.

While nitridation requires higher temperatures, 2D sulfides and selenides (e.g. GaS, SnS, and Bi_2Se_3) can be formed from 2DMOs at lower temperatures. For example, Carey et al. demonstrated liquid metal printing of n-type 2D GaS in 2017 using a 300 ºC tube furnace anneal with S powder preceded by conversion to $GaCl_3$[28]. The authors additionally demonstrated synthesis of In_2S_3 via bromination. 2D SnS has also been successfully synthesized by directly reacting the surface of molten Sn with H_2S gas at 350 ºC, followed by transfer via Van der Waals printing[111]. Liquid metal-derived p-type SnS materials exhibit high crystallinity, with large single crystal sheets visible by TEM as well as high hole mobility of 35 cm^2/Vs determined by Hall-effect measurements. Bi_2O_3 can also be converted via sulfurization, producing Bi_2S_3 with an optical bandgap of approximately 2.3 eV serving in photodetectors[135]. Similar to metal sulfides, metal

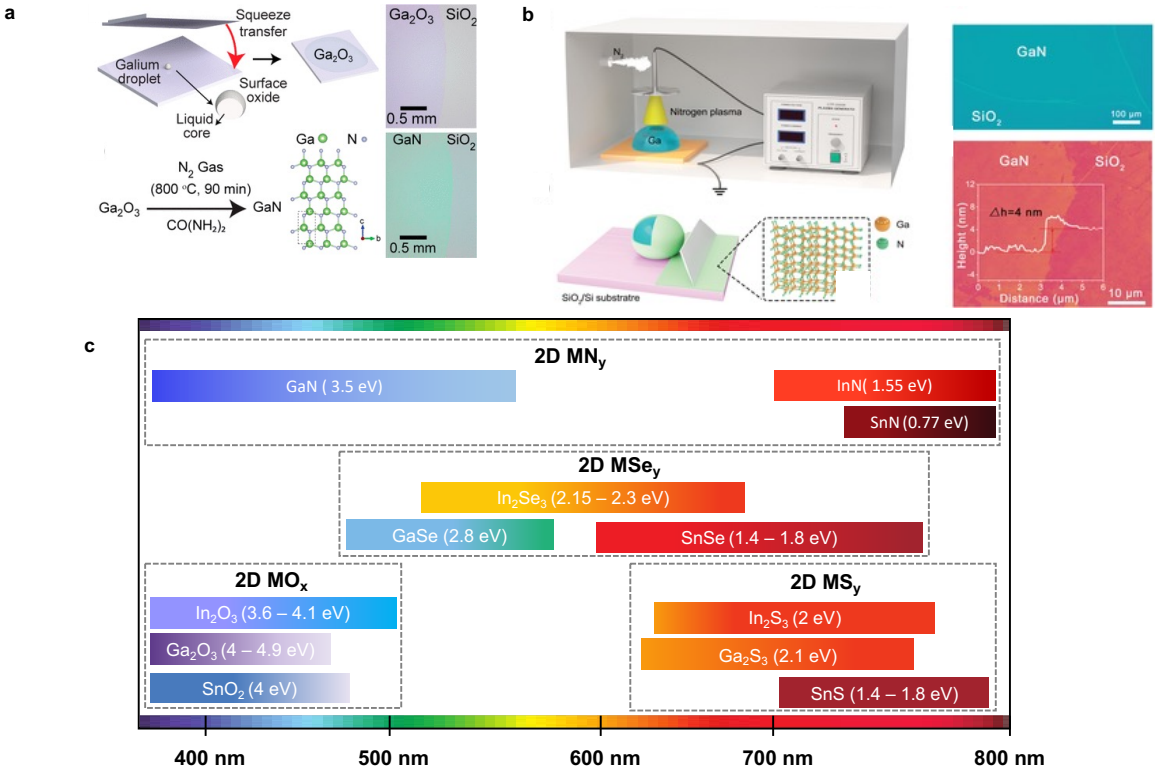

***Figure 12**: (a) Liquid metal synthesis and conversion of Ga_2O_3 into GaN via $CO(NH_2)_2$ annealed at 800 ºC. Reproduced from Ref.* [132]*. (b) Liquid metal synthesis of GaN films using nitrogen plasma (reproduced from Ref*[95]*). (c) Plot showing bandgap energy and wavelengths for optical absorption of 2D oxides (MO_x), 2D metal nitrides (MN_y), 2D metal selenides (MSe_y), and 2D metal sulfides (MS_y) synthesized from liquid metal interfaces.*

selenides can offer lower bandgaps for visible range responsivity. 2DMOs such as In_2O_3 can be converted to In_2Se_3 via a gas phase reaction with Se at 450 ºC in a tube furnace, resulting in a film with a bandgap of 1.92 eV[88]. In this work, Liao et al. also show that modulating the O_2 partial pressure (in an N_2 glovebox) for liquid metal printedIn_2O_3 films can be extended to control the resulting In_2Se_3 thickness. Further integration of liquid metal synthesized 2D In_2Se_3 can also leverage heterostructures with other 2D materials such as hexagonal boron nitride (h-BN) to encapsulate and stabilize In_2Se_3[136]. Likewise, liquid gallium surfaces can also seed the growth of large size single crystals of materials such as GaSe – with multiple authors claiming the role of the smooth liquid Ga surface in promoting the formation of large crystals[137].

The conversion of 2DMOs into 2D TMDs transforms them into visible range sensitive materials (E_g < 3 eV), as shown in the summary of the bandgaps of liquid metal-derived metal nitrides (MN_y), metal sulfides (MS_y), and metal selenides (MSe_y) provided in **Figure 12c**. Sn-based compounds in this series offer the greatest potential for designing infrared (IR) sensitive photodetectors or phototransistors. While liquid metal-derived 2D SnS has been demonstrated[111,131], SnSe and SnN both remain ideal targets for liquid metal-based synthesis of low bandgap materials. Additionally, these new families of 2D selenides, sulfides, and nitrides can offer properties such as piezoelectricity and ferroelectricity (e.g. α-In_2Se_3). Here we highlight specifically that 2DMOs offer the capability to stack and integrate large area heterostructures consisting of liquid metal-derived materials[9,13]. This provides an approach to go beyond the limitations of CVD growth or transfer methods widely used for transition metal dichalcogenides (TMDs). Despite their polycrystalline nature, liquid metal-derived 2D materials such as InN can demonstrate common heterostructure effects such as 2D electron gas (2DEG) formation more commonly associated with single crystal III-V materials and can exhibit electron mobility greater than 200 cm^2/Vs[138]. These properties suggest an opportunity for 2DMOs to propel a range of high-performance devices beyond the typical large area application set associated with printed electronic materials.

Ongoing scientific challenges for 2DMOs include understanding the thermodynamics and kinetics of doping. Doping is critical for engineering electrostatic control of new ternary and quaternary oxides (e.g. IZO, IGZO, etc.) but also for making high conductivity transparent electrodes. The influence of metal precursor stoichiometry will also be paramount to engineering the crystalline structure of 2DMOs and exploring the potential advantages of maintaining oxides

in the amorphous phase. For example, recent work studying fracture in glasses such as Al_2O_3 has shown a ductility of the amorphous phase that is beyond any expectations of ceramic materials[139]. Stoichiometric control of 2DMOs requires controlling the high level of surface enrichment of 'oxyphilic' metals that appear as a small percentages of the parent alloys[38]. In the case of certain high melting temperature metals such as HfO_2, this control will likely be paramount to growing oxides with unique properties (piezoelectric, ferroelectric[84], etc.). This is the main current disadvantage of 2DMOs relative to an alternative material system such as sol-gel-derived metal oxides. Sol-gel technique has free and near-deterministic control over doping in the resultant film whereas 2DMOs have a composition dependent on a loosely predictable combination of kinetics and thermodynamics. Overcoming this specific challenge will substantially broaden the material set of 2DMOs and lead to new functionality.

As 2DMOs are fundamentally ultrathin materials with properties determined by their *interfaces* – this means that characterizing their surface chemistry and structure is challenging but essential. Advanced nanoscale characterization and elemental mapping can help to address questions regarding the incorporation of dopants, for example, the possibility for phase segregation into nanoscale mixed phases[39] rather than substitutional doping. Advanced characterization methods must also be complemented by computational studies (e.g. *ab initio* molecular dynamics[39]), which could unlock deeper control and understanding of the Cabrera Mott process. The coupling between the electronic properties of oxides, the nanoscale growth mechanism, and the resultant morphologies and composition could be one of the most challenging scientific questions to unravel. The payoff, however, is the ability to access the near-infinite set of permutations offered by both doping and stacking of 2D oxides – a potential toolbox for the design of switching, memory, and sensing devices with programmable layer architectures.

In regard to fabrication, there is a great need for automated and repeatable methods for depositing 2DMOs. Few previous papers have demonstrated direct deposition of 2DMOs on flexible polymer substrates[13,59], though this is an important aim for the field since a distinguishing feature of 2DMOs is their low processing temperature capabilities. Overcoming challenges related to the planarity of polymer substrates and ensuring high adhesion should be a priority area going forward. These needs could drive the development of plasma-based methods for surface treatments to improve adhesion[13]. Sophisticated and precise methods for printing 2DMO multilayers and heterostructures can unlock new device applications if thickness can be controlled at the angstrom-level – but this requires stacking films with greater control. This has become essential because the field is at a level of maturity where repeatability is key to challenging more established material systems and to allow broader replication of results. Finally, a challenge that the field must address to compete with incumbent vacuum deposition methods is the ability to additively pattern. Methods that can truly be called printing should facilitate direct patterning[27] of 2DMOs without

the need for subtractive etching steps that reduce throughput and limit process integration. Expanding this laser-based transfer beyond GaO_x could offer new device integration possibilities.

4. Conclusion

This study has reviewed the key electronic and optoelectronic properties of an emerging class of 2D metal oxide (2DMO) materials, including their quantum-confined behavior, the influence of their interfaces and the passivation of those interfaces, and their crystallinity. We also probe the origins of these exceptional properties by considering the synthesis processes used to make 2D oxides based on Cabrera Mott surface oxidation and the mechanisms for controlling the deposited thickness. Opportunities for breakthrough advancements in patterning of 2D oxides as well as control over doping and stoichiometry are also reviewed. The methods recently demonstrated to convert 2DMOs into other families of 2D materials including metal sulfides, nitrides, and selenides have extended this scalable approach to high-performance materials with a variety of new applications. We provided a detailed review of device physics of switching devices based on 2DMOs in oxide electronics and the suitability of these materials as channel layers in high performance thin film transistors for both n-type and p-type operation and inverter circuit applications. Finally, this review highlighted recent advances in device integration for neuromorphic computing, gas sensing, photonic circuits, and photodetection applications of 2D oxides. Beyond these demonstrations, further research in this field can leverage the vast synthetic possibilities, large area scalability, and exceptionally high performance to power ambitious applications of 2DMOs across a broad spectrum of electronics and energy devices for next-generation electronics.

Supporting Information

Supporting Information is available from the Wiley Online Library including a table and figure showing the full lists of references included in Figure 10c.

Conflict of Interest

The authors declare no conflict of interest.

Data Availability Statement

Data sharing is not applicable to this article as no new data were created or analyzed in this study.

Acknowledgements

This research was supported by the National Science Foundation Electronic and Photonic Materials program (Award #2202501) as well as the National Science Foundation Electronics, Photonics, and Magnetic Devices program (Award #2219991).

Received: ((will be filled in by the editorial staff))
Revised: ((will be filled in by the editorial staff))
Published online: ((will be filled in by the editorial staff))

References

[1] A. Zavabeti, J. Z. Ou, B. J. Carey, N. Syed, R. Orrell-Trigg, E. L. H. Mayes, C. Xu, O. Kavehei, A. P. O'Mullane, R. B. Kaner, K. Kalantar-zadeh, T. Daeneke, *Science* **2017**, *358*, 332.

[2] R. S. Datta, N. Syed, A. Zavabeti, A. Jannat, M. Mohiuddin, M. Rokunuzzaman, B. Yue Zhang, M. A. Rahman, P. Atkin, K. A. Messalea, M. B. Ghasemian, E. D. Gaspera, S. Bhattacharyya, M. S. Fuhrer, S. P. Russo, C. F. McConville, D. Esrafilzadeh, K. Kalantar-Zadeh, T. Daeneke, *Nature Electronics* **2020**, *3*, 51.

[3] X. Guo, C. Kim Nguyen, A. Mazumder, Y. Wang, N. Syed, E. Della Gaspera, T. Daeneke, S. Walia, S. J. Ippolito, Y. Sabri, Y. Li, A. Zavabeti, *Nanoscale* **2023**, *15*, 4972.

[4] M. B. Ghasemian, A. Zavabeti, R. Abbasi, P. V. Kumar, N. Syed, Y. Yao, J. Tang, Y. Wang, A. Elbourne, J. Han, M. Mousavi, T. Daeneke, K. Kalantar-Zadeh, *Journal of Materials Chemistry A* **2020**, *8*, 19434.

[5] A. Zavabeti, B. Y. Zhang, I. A. de Castro, J. Z. Ou, B. J. Carey, M. Mohiuddin, RobiS. Datta, C. Xu, A. P. Mouritz, C. F. McConville, A. P. O'Mullane, T. Daeneke, K. Kalantar-Zadeh, *Advanced Functional Materials* **2018**, *28*, 1804057.

[6] A. B. Hamlin, Y. Ye, J. E. Huddy, M. S. Rahman, W. J. Scheideler, *npj 2D Mater Appl* **2022**, *6*, 1.

[7] Y. Ye, A. B. Hamlin, J. E. Huddy, M. S. Rahman, W. J. Scheideler, *Advanced Functional Materials* **2022**, *32*, 2204235.

[8] C. K. Nguyen, A. Mazumder, E. L. Mayes, V. Krishnamurthi, A. Zavabeti, B. J. Murdoch, X. Guo, P. Aukarasereenont, A. Dubey, A. Jannat, X. Wei, V. K. Truong, L. Bao, A. Roberts, C. F. McConville, S. Walia, N. Syed, T. Daeneke, *Advanced Materials Interfaces* **n.d.**, *n/a*, 2202036.

[9] M. M. Y. A. Alsaif, S. Kuriakose, S. Walia, N. Syed, A. Jannat, B. Y. Zhang, F. Haque, M. Mohiuddin, T. Alkathiri, N. Pillai, T. Daeneke, J. Z. Ou, A. Zavabeti, *Advanced Materials Interfaces* **2019**, *6*, 1900007.

[10] A. Zavabeti, P. Aukarasereenont, H. Tuohey, N. Syed, A. Jannat, A. Elbourne, K. A. Messalea, B. Y. Zhang, B. J. Murdoch, J. G. Partridge, M. Wurdack, D. L. Creedon, J. van Embden, K. Kalantar-Zadeh, S. P. Russo, C. F. McConville, T. Daeneke, *Nat Electron* **2021**, *4*, 277.

[11] C.-H. Huang, Y. Tang, T.-Y. Yang, Y.-L. Chueh, K. Nomura, *ACS Appl. Mater. Interfaces* **2021**, *13*, 52783.

[12] A. Zavabeti, J. Z. Ou, B. J. Carey, N. Syed, R. Orrell-Trigg, E. L. H. Mayes, C. Xu, O. Kavehei, A. P. O'Mullane, R. B. Kaner, K. Kalantar-zadeh, T. Daeneke, *Science* **2017**, *358*, 332.

[13] Y. Ye, A. B. Hamlin, J. E. Huddy, M. S. Rahman, W. J. Scheideler, *Advanced Functional Materials* **2022**, *32*, 2204235.

[14] Y. Li, S. Yin, Y. Du, H. Zhang, J. Chen, Z. Wang, S. Wang, Q. Qin, M. Zhou, L. Li, *Nanoscale* **2022**, *14*, 16797.

[15] C. K. Nguyen, A. Mazumder, E. L. Mayes, V. Krishnamurthi, A. Zavabeti, B. J. Murdoch, X. Guo, P. Aukarasereenont, A. Dubey, A. Jannat, X. Wei, V. K. Truong, L. Bao, A. Roberts, C. F. McConville, S. Walia, N. Syed, T. Daeneke, *Advanced Materials Interfaces* **2023**, *10*, 2202036.

[16] K. A. Messalea, N. Syed, A. Zavabeti, M. Mohiuddin, A. Jannat, P. Aukarasereenont, C. K. Nguyen, M. X. Low, S. Walia, B. Haas, C. T. Koch, N. Mahmood, K. Khoshmanesh, K. Kalantar-Zadeh, T. Daeneke, *ACS Nano* **2021**, *15*, 16067.

[17] M. Karbalaei Akbari, F. Verpoort, S. Zhuiykov, *Applied Materials Today* **2022**, *27*, 101461.

[18] N. Syed, A. Zavabeti, J. Z. Ou, M. Mohiuddin, N. Pillai, B. J. Carey, B. Y. Zhang, R. S. Datta, A. Jannat, F. Haque, K. A. Messalea, C. Xu, S. P. Russo, C. F. McConville, T. Daeneke, K. Kalantar-Zadeh, *Nat Commun* **2018**, *9*, 3618.

[19] N. Syed, A. Stacey, A. Zavabeti, C. K. Nguyen, B. Haas, C. T. Koch, D. L. Creedon, E. Della Gaspera, P. Reineck, A. Jannat, M. Wurdack, S. E. Bamford, P. J. Pigram, S. A. Tawfik, S. P. Russo, B. J. Murdoch, K. Kalantar-Zadeh, C. F. McConville, T. Daeneke, *ACS Nano* **2022**, *16*, 5476.

[20] A. B. Hamlin, S. A. Agnew, J. C. Bonner, J. W. P. Hsu, W. J. Scheideler, *Nano Lett.* **2023**, *23*, 2544.

[21] W. H. Organization, I. P. on C. Safety, *2-Methoxyethanol, 2-Ethoxyethanol and Their Acetates*, World Health Organization, **1990**.

[22] W. Scheideler, V. Subramanian, *Nanotechnology* **2019**, *30*, 272001.

[23] Y. Ye, A. B. Hamlin, J. E. Huddy, M. S. Rahman, W. J. Scheideler, *Advanced Functional Materials* **2022**, *32*, 2204235.

[24] Q. Li, J. Lin, T.-Y. Liu, X.-Y. Zhu, W.-H. Yao, J. Liu, *npj 2D Mater Appl* **2021**, *5*, 1.

[25] A. B. Hamlin, Y. Ye, J. E. Huddy, M. S. Rahman, W. J. Scheideler, *npj 2D Mater Appl* **2022**, *6*, 1.

[26] Y. Huang, E. Sutter, N. N. Shi, J. Zheng, T. Yang, D. Englund, H.-J. Gao, P. Sutter, *ACS Nano* **2015**, *9*, 10612.

[27] L. An, D. de C. Branco, X. Liu, H. Jiang, M. Wang, J. Xu, R. Zhang, W. Wu, G. J. Cheng, *Matter* **2023**, *6*, 1203.

[28] B. J. Carey, J. Z. Ou, R. M. Clark, K. J. Berean, A. Zavabeti, A. S. R. Chesman, S. P. Russo, D. W. M. Lau, Z.-Q. Xu, Q. Bao, O. Kavehei, B. C. Gibson, M. D. Dickey, R. B. Kaner, T. Daeneke, K. Kalantar-Zadeh, *Nat Commun* **2017**, *8*, 14482.

[29] K. Xing, P. Aukarasereenont, S. Rubanov, A. Zavabeti, D. L. Creedon, W. Li, B. C. Johnson, C. I. Pakes, J. C. McCallum, T. Daeneke, D.-C. Qi, *ACS Appl. Electron. Mater.* **2022**, *4*, 2272.

[30] A. C. Arias, J. D. MacKenzie, I. McCulloch, J. Rivnay, A. Salleo, *Chem. Rev.* **2010**, *110*, 3.

[31] Y. S. Rim, H. Chen, T.-B. Song, S.-H. Bae, Y. Yang, *Chem. Mater.* **2015**, *27*, 5808.

[32] W. J. Scheideler, R. Kumar, A. R. Zeumault, V. Subramanian, *Advanced Functional Materials* **2017**, *27*, 1606062.

[33] J. Leppäniemi, O.-H. Huttunen, H. Majumdar, A. Alastalo, *Advanced Materials* **2015**, *27*, 7168.

[34] B. Wang, P. Guo, L. Zeng, X. Yu, A. Sil, W. Huang, M. J. Leonardi, X. Zhang, G. Wang, S. Lu, Z. Chen, M. J. Bedzyk, R. D. Schaller, T. J. Marks, A. Facchetti, *PNAS* **2019**, *116*, 9230.

[35] J. T. Gudmundsson, *Plasma Sources Sci. Technol.* **2020**, *29*, 113001.

[36] S. I. Bakhtiyarov, R. A. Overfelt, *Acta Materialia* **1999**, *47*, 4311.

[37] V. Zardetto, T. M. Brown, A. Reale, A. Di Carlo, *Journal of Polymer Science Part B: Polymer Physics* **2011**, *49*, 638.

[38] Z. J. Farrell, A. R. Jacob, V. K. Truong, A. Elbourne, W. Kong, L. Hsiao, M. D. Dickey, C. Tabor, *Chem. Mater.* **2023**, *35*, 964.

[39] M. B. Ghasemian, A. Zavabeti, M. Mousavi, B. J. Murdoch, A. J. Christofferson, N. Meftahi, J. Tang, J. Han, R. Jalili, F.-M. Allioux, M. Mayyas, Z. Chen, A. Elbourne, C. F. McConville, S. P. Russo, S. Ringer, K. Kalantar-Zadeh, *Advanced Materials* **2021**, *33*, 2104793.

[40] I. D. Joshipura, K. A. Persson, V. K. Truong, J.-H. Oh, M. Kong, M. H. Vong, C. Ni, M. Alsafatwi, D. P. Parekh, H. Zhao, M. D. Dickey, *Langmuir* **2021**, *37*, 10914.

[41] S. Boandoh, F. O.-T. Agyapong-Fordjour, S. H. Choi, J. S. Lee, J.-H. Park, H. Ko, G. Han, S. J. Yun, S. Park, Y.-M. Kim, W. Yang, Y. H. Lee, S. M. Kim, K. K. Kim, *ACS Appl. Mater. Interfaces* **2019**, *11*, 1579.

[42] D. W. G. White, *Metall Trans* **1972**, *3*, 1933.

[43] S. Handschuh-Wang, T. Gan, T. Wang, F. J. Stadler, X. Zhou, *Langmuir* **2021**, *37*, 9017.

[44] Z. Yuan, J. Fan, J. Li, J. Ke, K. Mukai, *Scandinavian Journal of Metallurgy* **2004**, *33*, 338.

[45] Y. Plevachuk, V. Sklyarchuk, S. Eckert, G. Gerbeth, R. Novakovic, *J. Chem. Eng. Data* **2014**, *59*, 757.

[46] A. Passerone, E. Ricci, R. Sangiorgi, *J Mater Sci* **1990**, *25*, 4266.

[47] S. C. Hardy, *Journal of Crystal Growth* **1985**, *71*, 602.

[48] D. Giuranno, F. Gnecco, E. Ricci, R. Novakovic, *Intermetallics* **2003**, *11*, 1313.

[49] J. N. Koster, *Crystal Research and Technology* **1999**, *34*, 1129.
[50] L. Zhu, B. Wang, S. Handschuh-Wang, X. Zhou, *Small* **2020**, *16*, 1903841.
[51] Y. Tang, C.-H. Huang, K. Nomura, *ACS Nano* **2022**, *16*, 3280.
[52] P. Atkin, R. Orrell-Trigg, A. Zavabeti, N. Mahmood, M. R. Field, T. Daeneke, I. S. Cole, K. Kalantar-zadeh, *Chemical Communications* **2018**, *54*, 2102.
[53] H. Wang, S. Chen, X. Zhu, B. Yuan, X. Sun, J. Zhang, X. Yang, Y. Wei, J. Liu, *Matter* **2022**, *5*, 2054.
[54] D. D. Williams, R. R. Miller, *J. Am. Chem. Soc.* **1950**, *72*, 3821.
[55] Z. Liu, Y. Bando, M. Mitome, J. Zhan, *Phys. Rev. Lett.* **2004**, *93*, 095504.
[56] X. Guo, C. K. Nguyen, N. Syed, A. Ravindran, M. A. Islam, T. Filleter, K. Cao, Y. Wang, A. Mazumder, C. Xu, S. Walia, M. B. Ghasemian, K. Kalantar-Zadeh, S. C. Scholten, I. O. Robertson, A. J. Healey, J.-P. Tetienne, T. Lu, Y. Liu, A. Elbourne, T. Daeneke, A. Holland, S. P. Russo, Y. Li, A. Zavabeti, *Advanced Functional Materials* **n.d.**, *n/a*, 2307348.
[57] J. Ma, F. Krisnadi, M. H. Vong, M. Kong, O. M. Awartani, M. D. Dickey, *Advanced Materials* **2023**, *35*, 2205196.
[58] T. V. Neumann, M. D. Dickey, *Advanced Materials Technologies* **2020**, *5*, 2000070.
[59] R. S. Datta, N. Syed, A. Zavabeti, A. Jannat, M. Mohiuddin, M. Rokunuzzaman, B. Yue Zhang, M. A. Rahman, P. Atkin, K. A. Messalea, M. B. Ghasemian, E. D. Gaspera, S. Bhattacharyya, M. S. Fuhrer, S. P. Russo, C. F. McConville, D. Esrafilzadeh, K. Kalantar-Zadeh, T. Daeneke, *Nat Electron* **2020**, *3*, 51.
[60] N. Cabrera, N. F. Mott, *Rep. Prog. Phys.* **1949**, *12*, 163.
[61] L. P. Ramírez, F. Bournel, J.-J. Gallet, L. Dudy, F. Rochet, *J. Phys. Chem. C* **2022**, *126*, 2517.
[62] Y. Tang, C.-H. Huang, K. Nomura, *ACS Nano* **2022**, *16*, 3280.
[63] A. Jannat, N. Syed, K. Xu, Md. A. Rahman, Md. M. M. Talukder, K. A. Messalea, Md. Mohiuddin, R. S. Datta, M. W. Khan, T. Alkathiri, B. J. Murdoch, S. Z. Reza, J. Li, T. Daeneke, A. Zavabeti, J. Z. Ou, *ACS Nano* **2021**, *15*, 4045.
[64] C. K. Nguyen, M. X. Low, A. Zavabeti, B. J. Murdoch, X. Guo, P. Aukarasereenont, A. Mazumder, A. Dubey, A. Jannat, Md. A. Rahman, K. Chiang, V. K. Truong, L. Bao, C. F. McConville, S. Walia, T. Daeneke, N. Syed, *Advanced Optical Materials* **2022**, *10*, 2200925.
[65] A. Goff, P. Aukarasereenont, C. K. Nguyen, R. Grant, N. Syed, A. Zavabeti, A. Elbourne, T. Daeneke, *Dalton Transactions* **2021**, *50*, 7513.
[66] M. Si, Y. Hu, Z. Lin, X. Sun, A. Charnas, D. Zheng, X. Lyu, H. Wang, K. Cho, P. D. Ye, *Nano Lett.* **2021**, *21*, 500.
[67] M. Xie, X. Sun, S. M. George, C. Zhou, J. Lian, Y. Zhou, *ACS Appl. Mater. Interfaces* **2015**, *7*, 27735.

[68] L. P. H. Jeurgens, W. G. Sloof, F. D. Tichelaar, E. J. Mittemeijer, *Phys. Rev. B* **2000**, *62*, 4707.
[69] F. Reichel, L. P. H. Jeurgens, E. J. Mittemeijer, *Acta Materialia* **2008**, *56*, 659.
[70] A. G. Kelly, D. O'Suilleabhain, C. Gabbett, J. N. Coleman, *Nat Rev Mater* **2022**, *7*, 217.
[71] Y. Magari, T. Kataoka, W. Yeh, M. Furuta, *Nat Commun* **2022**, *13*, 1078.
[72] A. Zavabeti, P. Aukarasereenont, H. Tuohey, N. Syed, A. Jannat, A. Elbourne, K. A. Messalea, B. Y. Zhang, B. J. Murdoch, J. G. Partridge, M. Wurdack, D. L. Creedon, J. van Embden, K. Kalantar-Zadeh, S. P. Russo, C. F. McConville, T. Daeneke, *Nat Electron* **2021**, *4*, 277.
[73] B. Macco, M. A. Verheijen, L. E. Black, B. Barcones, J. Melskens, W. M. M. Kessels, *Journal of Applied Physics* **2016**, *120*, 085314.
[74] Z. Hu, T. Yuan, H. Li, Y. Qiu, W. Zhou, J. Zhang, Y. Zhao, S. Hu, *Nano Res.* **2021**, *14*, 4795.
[75] N. Syed, C. K. Nguyen, A. Zavabeti, M. X. Low, X. Wei, V. Krishnamurthi, M. Irfan, W. S. L. Lee, N. M. H. Duong, A. T. Nguyen, P. Reineck, L. Bao, A. Roberts, T. Daeneke, *ACS Appl. Electron. Mater.* **2024**, DOI 10.1021/acsaelm.3c01842.
[76] M. D. Dickey, R. C. Chiechi, R. J. Larsen, E. A. Weiss, D. A. Weitz, G. M. Whitesides, *Advanced Functional Materials* **2008**, *18*, 1097.
[77] J. Cooke, L. Ghadbeigi, R. Sun, A. Bhattacharyya, Y. Wang, M. A. Scarpulla, S. Krishnamoorthy, B. Sensale-Rodriguez, *physica status solidi (a)* **2020**, *217*, 1901007.
[78] Y. Xu, J. Zhang, X. Han, X. Wang, C. Ye, W. Mu, Z. Jia, K. Qian, *ACS Appl. Mater. Interfaces* **2023**, *15*, 25831.
[79] R. Lin, W. Zheng, D. Zhang, Y. Li, F. Huang, *ACS Appl. Electron. Mater.* **2019**, *1*, 2166.
[80] M. J. Regan, H. Tostmann, P. S. Pershan, O. M. Magnussen, E. DiMasi, B. M. Ocko, M. Deutsch, *Phys. Rev. B* **1997**, *55*, 10786.
[81] J. Li, X. Zhang, B. Yang, C. Zhang, T. Xu, L. Chen, L. Yang, X. Jin, B. Liu, *Chem. Mater.* **2021**, *33*, 4568.
[82] J. Cutinho, B. S. Chang, S. Oyola-Reynoso, J. Chen, S. S. Akhter, I. D. Tevis, N. J. Bello, A. Martin, M. C. Foster, M. M. Thuo, *ACS Nano* **2018**, *12*, 4744.
[83] Q. Liu, J. Guo, J. Li, L. Feng, L. Chen, Z. Hua, L. Yang, X. Zhang, B. Liu, *ACS Appl. Nano Mater.* **2023**, *6*, 3027.
[84] M. B. Ghasemian, A. Zavabeti, F.-M. Allioux, P. Sharma, M. Mousavi, Md. A. Rahim, R. Khayyam Nekouei, J. Tang, A. J. Christofferson, N. Meftahi, S. Rafiezadeh, S. Cheong, P. Koshy, R. D. Tilley, C. F. McConville, S. P. Russo, C. Ton-That, J. Seidel, K. Kalantar-Zadeh, *Small* **n.d.**, *n/a*, 2309924.
[85] P. H. A. Vaillant, V. Krishnamurthi, C. J. Parker, R. Kariuki, S. P. Russo, A. J. Christofferson, T. Daeneke, A. Elbourne, *Advanced Functional Materials* **n.d.**, *n/a*, 2310147.

[86] B. Du, Q. Li, X. Meng, J. Liu, *ACS Appl. Electron. Mater.* **2023**, *5*, 1879.
[87] X. Chen, B. Du, Q. Li, J. Liu, *Journal of Alloys and Compounds* **2024**, *976*, 173077.
[88] B. Liao, H. Shen, H. Zhu, B. Gao, Z. Wang, J. Zhang, W. Mao, Y. Li, T. Wu, *ACS Appl. Electron. Mater.* **2023**, *5*, 1088.
[89] M. Si, Y. Hu, Z. Lin, X. Sun, A. Charnas, D. Zheng, X. Lyu, H. Wang, K. Cho, P. D. Ye, *Nano Lett.* **2021**, *21*, 500.
[90] D.-H. Lee, S.-M. Park, D.-K. Kim, Y.-S. Lim, M. Yi, *JOURNAL OF SEMICONDUCTOR TECHNOLOGY AND SCIENCE* **2014**, *14*, 163.
[91] Y. G. Kim, T. Kim, C. Avis, S.-H. Lee, J. Jang, *IEEE Transactions on Electron Devices* **2016**, *63*, 1078.
[92] Y. Tang, K. Nomura, *ECS Meeting Abstracts* **2022**, *2022*, 2557.
[93] C. Kim Nguyen, M. Xian Low, A. Zavabeti, A. Jannat, B. J. Murdoch, E. D. Gaspera, R. Orrell-Trigg, S. Walia, A. Elbourne, V. Khanh Truong, C. F. McConville, N. Syed, T. Daeneke, *Journal of Materials Chemistry C* **2021**, *9*, 11815.
[94] B. Du, Q. Li, J. Wei, J. Liu, *ACS Appl. Nano Mater.* **2023**, DOI 10.1021/acsanm.3c03362.
[95] Q. Li, B.-D. Du, J.-Y. Gao, B.-Y. Xing, D.-K. Wang, J.-F. Ye, J. Liu, *Advanced Materials Technologies* **2022**, *7*, 2200733.
[96] M. M. Y. A. Alsaif, N. Pillai, S. Kuriakose, S. Walia, A. Jannat, K. Xu, T. Alkathiri, M. Mohiuddin, T. Daeneke, K. Kalantar-Zadeh, J. Z. Ou, A. Zavabeti, *ACS Appl. Nano Mater.* **2019**, *2*, 4665.
[97] H. H. Choi, K. Cho, C. D. Frisbie, H. Sirringhaus, V. Podzorov, *Nature Mater* **2018**, *17*, 2.
[98] X. Wang, A. Dodabalapur, *IEEE Transactions on Electron Devices* **2021**, *68*, 125.
[99] X. Wang, A. Dodabalapur, *Annalen der Physik* **2018**, *530*, 1800341.
[100] J. F. Wager, *Journal of the Society for Information Display* **2023**, *31*, 608.
[101] W. Xu, H. Li, J.-B. Xu, L. Wang, *ACS Appl. Mater. Interfaces* **2018**, *10*, 25878.
[102] J. F. Wager, B. Yeh, R. L. Hoffman, D. A. Keszler, *Current Opinion in Solid State and Materials Science* **2014**, *18*, 53.
[103] M. Gebert, S. Bhattacharyya, C. C. Bounds, N. Syed, T. Daeneke, M. S. Fuhrer, *Nano Lett.* **2023**, *23*, 363.
[104] Y. Zhang, D. Venkatakrishnarao, M. Bosman, W. Fu, S. Das, F. Bussolotti, R. Lee, S. L. Teo, D. Huang, I. Verzhbitskiy, Z. Jiang, Z. Jiang, J. Chai, S. W. Tong, Z.-E. Ooi, C. P. Y. Wong, Y. S. Ang, K. E. J. Goh, C. S. Lau, *ACS Nano* **2023**, *17*, 7929.
[105] A. M. Reddy, A. S. Reddy, P. S. Reddy, *Physics Procedia* **2013**, *49*, 9.
[106] J. Jo, J. D. Lenef, K. Mashooq, O. Trejo, N. P. Dasgupta, R. L. Peterson, *IEEE Transactions on Electron Devices* **2020**, *67*, 5557.

[107] M. Filella, C. Reimann, M. Biver, I. Rodushkin, K. Rodushkina, *Environ. Chem.* **2019**, *16*, 215.

[108] A. Taylor, *Biol Trace Elem Res* **1996**, *55*, 231.

[109] C.-H. Huang, Y. Tang, T.-Y. Yang, Y.-L. Chueh, K. Nomura, *ACS Appl. Mater. Interfaces* **2021**, *13*, 52783.

[110] K. Huang, L. Guo, L. Liu, X. Chen, C. Su, P. Li, Z. Deng, W. Wu, L. Zhang, *Journal of Materials Chemistry C* **2023**, DOI 10.1039/D3TC02405A.

[111] V. Krishnamurthi, H. Khan, T. Ahmed, A. Zavabeti, S. A. Tawfik, S. K. Jain, M. J. S. Spencer, S. Balendhran, K. B. Crozier, Z. Li, L. Fu, M. Mohiuddin, M. X. Low, B. Shabbir, A. Boes, A. Mitchell, C. F. McConville, Y. Li, K. Kalantar-Zadeh, N. Mahmood, S. Walia, *Advanced Materials* **2020**, *32*, 2004247.

[112] D. Tordera, B. Peeters, H. B. Akkerman, A. J. J. M. van Breemen, J. Maas, S. Shanmugam, A. J. Kronemeijer, G. H. Gelinck, *Advanced Materials Technologies* **2019**, *4*, 1900651.

[113] S. Wei, F. Wang, X. Zou, L. Wang, C. Liu, X. Liu, W. Hu, Z. Fan, J. C. Ho, L. Liao, *Advanced Materials* **2020**, *32*, 1907527.

[114] Y. Zhang, B. Gao, D. Lepage, Y. Tong, P. Wang, W. Xia, J. Niu, Y. Feng, H. Chen, H. Qian, *Nat. Nanotechnol.* **2024**, *19*, 463.

[115] M. Karbalaei Akbari, F. Verpoort, S. Zhuiykov, *Applied Materials Today* **2022**, *27*, 101461.

[116] C.-H. Huang, C.-Y. Weng, K.-H. Chen, Y. Chou, T.-L. Wu, Y.-C. Chou, *ACS Appl. Mater. Interfaces* **2023**, *15*, 25838.

[117] C.-H. Huang, H. Chang, T.-Y. Yang, Y.-C. Wang, Y.-L. Chueh, K. Nomura, *ACS Appl. Mater. Interfaces* **2021**, *13*, 52822.

[118] A. Mazumder, C. K. Nguyen, T. Aung, M. X. Low, Md. A. Rahman, S. P. Russo, S. A. Tawfik, S. Wang, J. Bullock, V. Krishnamurthi, N. Syed, A. Ranjan, A. Zavabeti, I. H. Abidi, X. Guo, Y. Li, T. Ahmed, T. Daeneke, A. Al-Hourani, S. Balendhran, S. Walia, *Advanced Functional Materials* **n.d.**, *n/a*, 2303641.

[119] M. D. H. Chowdhury, P. Migliorato, J. Jang, *Applied Physics Letters* **2010**, *97*, 173506.

[120] T. Ahmed, A. Jannat, V. Krishnamurthi, T. Aung, A. Mazumder, A. Zavabeti, N. Syed, T. Daeneke, J. Z. Ou, A. AI-Hourani, S. Walia, *Advanced Materials Technologies* **2023**, *8*, 2201772.

[121] A. Mazumder, C. K. Nguyen, I. H. Abidi, A. Ranjan, T. Daeneke, T. Ahmed, S. Balendhran, S. Walia, *ACS Appl. Nano Mater.* **2024**, *7*, 1845.

[122] J. E. Huddy, M. S. Rahman, A. B. Hamlin, Y. Ye, W. J. Scheideler, *Cell Reports Physical Science* **2022**, *3*, 100786.

[123] Y. Cheng, Z. Li, L. Cheng, Y. Yuan, E. Xie, X. Cao, Z. Xin, Y. Liu, T. Tang, X. Hu, K. Xu, C. Manh Hung, A. Jannat, Y. X. Li, H. Chen, J. Z. Ou, *ACS Appl. Mater. Interfaces* **2023**, *15*, 57496.

[124] K. S. Kim, C. H. Ahn, S. H. Jung, S. W. Cho, H. K. Cho, *ACS Appl. Mater. Interfaces* **2018**, *10*, 10185.

[125] H. Tang, Y. Li, R. Sokolovskij, L. Sacco, H. Zheng, H. Ye, H. Yu, X. Fan, H. Tian, T.-L. Ren, G. Zhang, *ACS Appl. Mater. Interfaces* **2019**, *11*, 40850.

[126] C. K. Nguyen, P. D. Taylor, A. Zavabeti, H. Alluhaybi, S. Almalki, X. Guo, M. Irfan, M. A. Kobaisi, S. J. Ippolito, M. J. S. Spencer, S. Balendhran, A. Roberts, T. Daeneke, K. B. Crozier, Y. Sabri, N. Syed, *Advanced Functional Materials* **n.d.**, *n/a*, 2309342.

[127] Y. Chen, Z. Li, T. Tang, Y. Cheng, L. Cheng, X. Wang, A. A. Haidry, A. Jannat, J. Z. Ou, *ACS Appl. Nano Mater.* **2024**, *7*, 3229.

[128] M. Mousavi, M. B. Ghasemian, J. Han, Y. Wang, R. Abbasi, J. Yang, J. Tang, S. A. Idrus-Saidi, X. Guan, M. J. Christoe, S. Merhebi, C. Zhang, J. Tang, R. Jalili, T. Daeneke, T. Wu, K. Kalantar-Zadeh, M. Mayyas, *Applied Materials Today* **2021**, *22*, 100954.

[129] H.-W. Zan, C.-H. Li, C.-C. Yeh, M.-Z. Dai, H.-F. Meng, C.-C. Tsai, *Applied Physics Letters* **2011**, *98*, 253503.

[130] S. Knobelspies, B. Bierer, A. Daus, A. Takabayashi, G. A. Salvatore, G. Cantarella, A. Ortiz Perez, J. Wöllenstein, S. Palzer, G. Tröster, *Sensors* **2018**, *18*, 358.

[131] H. Khan, N. Mahmood, A. Zavabeti, A. Elbourne, M. A. Rahman, B. Y. Zhang, V. Krishnamurthi, P. Atkin, M. B. Ghasemian, J. Yang, G. Zheng, A. R. Ravindran, S. Walia, L. Wang, S. P. Russo, T. Daeneke, Y. Li, K. Kalantar-Zadeh, *Nat Commun* **2020**, *11*, 3449.

[132] N. Syed, A. Zavabeti, K. A. Messalea, E. Della Gaspera, A. Elbourne, A. Jannat, M. Mohiuddin, B. Y. Zhang, G. Zheng, L. Wang, S. P. Russo, D. Esrafilzadeh, C. F. McConville, K. Kalantar-Zadeh, T. Daeneke, *J. Am. Chem. Soc.* **2019**, *141*, 104.

[133] Y. Du, S. Yin, Y. Li, J. Chen, D. Shi, E. Guo, H. Zhang, Z. Wang, Q. Qin, C. Zou, T. Zhai, L. Li, *Small Methods* **n.d.**, *n/a*, 2300175.

[134] P. Pedram, A. Zavabeti, N. Syed, A. Slassi, C. K. Nguyen, B. Fornacciari, A. Lamirand, J. Galipaud, A. Calzolari, A. Boes, T. Daenke, S. Cueff, A. Mitchell, C. Monat, in *2D Photonic Materials and Devices VI*, SPIE, **2023**, pp. 35–41.

[135] K. A. Messalea, A. Zavabeti, M. Mohiuddin, N. Syed, A. Jannat, P. Atkin, T. Ahmed, S. Walia, C. F. McConville, K. Kalantar-Zadeh, N. Mahmood, K. Khoshmanesh, T. Daeneke, *Advanced Materials Interfaces* **2020**, *7*, 2001131.

[136] B. Gao, H. Zhu, C. Zhang, Z. Shi, S. Wang, W. Yin, T. Wu, *ACS Appl. Nano Mater.* **2023**, *6*, 19867.

[137] Z. Chen, Q. Chen, Z. Chai, B. Wei, J. Wang, Y. Liu, Y. Shi, Z. Wang, J. Li, *Nano Res.* **2022**, *15*, 4677.

[138] N. Syed, A. Stacey, A. Zavabeti, C. K. Nguyen, B. Haas, C. T. Koch, D. L. Creedon, E. Della Gaspera, P. Reineck, A. Jannat, M. Wurdack, S. E. Bamford, P. J. Pigram, S. A. Tawfik, S. P. Russo, B. J. Murdoch, K. Kalantar-Zadeh, C. F. McConville, T. Daeneke, *ACS Nano* **2022**, *16*, 5476.

[139] E. J. Frankberg, J. Kalikka, F. García Ferré, L. Joly-Pottuz, T. Salminen, J. Hintikka, M. Hokka, S. Koneti, T. Douillard, B. Le Saint, P. Kreiml, M. J. Cordill, T. Epicier, D. Stauffer, M. Vanazzi, L. Roiban, J. Akola, F. Di Fonzo, E. Levänen, K. Masenelli-Varlot, *Science* **2019**, *366*, 864.

Supporting Information

Advances in Liquid Metal Printed 2D Oxide Electronics

William J. Scheideler[1] and Kenji Nomura[2]*

[1]Thayer School of Engineering
Dartmouth College, Hanover, NH 03755, United States
E-mail: william.j.scheideler@dartmouth.edu

[2]Department of Electrical and Computer Engineering,
University of California San Diego, La Jolla, CA 92093, United States;

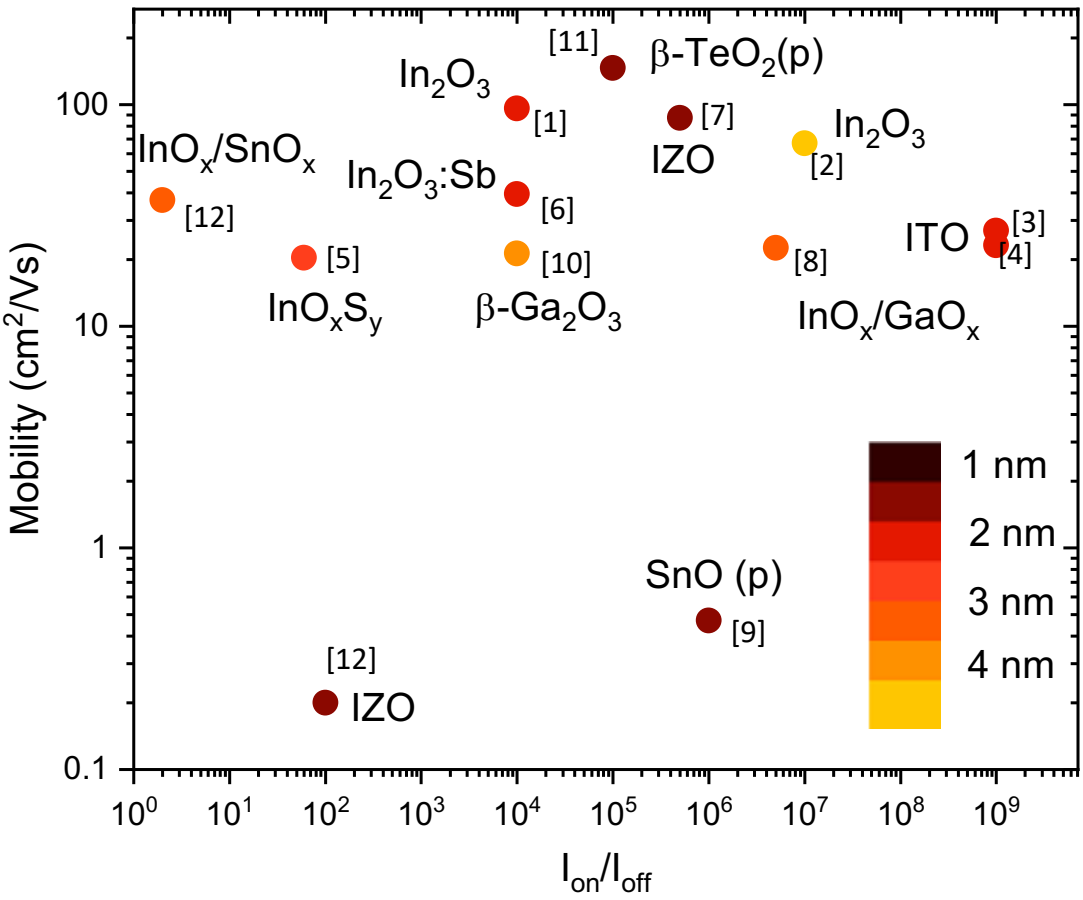

Figure S1: Figure 9a with annotations to indicate references cited for each data point. Plot shows mobility reported as a function of I_{on}/I_{off} ratio.

Table S1: References corresponding to Figure S2 for mobility and I_{on}/I_{off} of liquid metal printed semiconductors.

Reference	DOI
[1]	10.1002/admi.202202036
[2]	10.1038/s41699-022-00294-9
[3]	10.1021/acsnano.1c11205
[4]	10.1149/MA2022-02382557mtgabs
[5]	10.1002/admi.2019000007
[6]	10.1002/adom.202200925
[7]	10.1021/acsnano.0c06791
[8]	10.1021/acs.nanolett.2c04555
[9]	10.1021/acsami.1c15990
[10]	10.1002/pssr.201900271
[11]	10.1038/s41928-021-00606-9
[12]	10.1039/D2NR04535D